Fluid and Mineral Carbonate Biogeochemistry and Microbial Mats of Caribou Plateau Alkaline Lakes

by

Maya Olivia Thompson

A Thesis Submitted in Partial Fulfillment of the
Requirements of the

HONOURS PROGRAM

in the School of Earth and Ocean Sciences

Supervisor: Anne-Sofie Ahm

University of Victoria

We acknowledge and respect the Lək̓ʷəŋən (Songhees and Xʷsepsəm/Esquimalt) Peoples on whose territory the university stands, and the Lək̓ʷəŋən and W̱SÁNEĆ Peoples whose historical relationships with the land continue to this day.

THESIS

Fluid and mineral carbonate biogeochemistry and microbial mats of Caribou Plateau alkaline lakes

Maya O. Thompson*

[1]School of Earth and Ocean Sciences, University of Victoria, British Columbia, Canada

Correspondence
*M. O. Thompson, Email: m.0.thmpson@gmail.com

Abstract

Alkaliphilic microbial mats are the biological foundation in Interior British Columbia alkaline lakes. They are also associated with rare and hard-to-form carbonates that precipitate within the mat laminae. When analyzed with SEM, rounded mineral nodules and crystals were found growing along the length of fibrous microbial mat algaes. Mg-Ca minerals were also found on encrusted soil samples taken along the lacustrine shore. The storage of microbial mats in 90% EtOH shined a light on the importance of organic solvents in the precipitation of hard-to-form carbonates, as these samples were found to precipitate out Mg-Ca and Mg-Na minerals more readily than samples stored in other solutions. The changes in water samples combined with microenvironments created near cell walls suggest that a combination of high alkalinity and biological activities control the precipitation of hard-to-form carbonates. We seek to investigate the functions of microbial mats from a geologist's perspective and to couple it with in-lab experimentation and analysis, and computational modeling.

KEYWORDS:
Alkaline lake, microbially mediated precipitation, biogeochemistry, Mg-carbonate, alkaliphile

1 | INTRODUCTION

Alkaline lakes (also called 'soda lakes') are fixed bodies of water characterized by high pH and/or high carbonate alkalinity. They contain high concentrations of dissolved inorganic carbon (DIC) in the form of carbonate salts, in addition to other dissolved salts, resulting in hypersalinity. They are considered an extreme aquatic environment as they are too caustic and saline for most fauna and flora to survive. These chemical properties arise due to evaporation and the concentration of chemical analytes from inflowing source water. Despite their extreme chemistry and high pH and alkalinity, alkaline lakes are incredibly productive environments. Primary production along the surface of the lake is effectively infinite due to a functionally limitless amount of DIC, leading to some of the world's most efficient carbon draw-down and storage. However, the presence of a strong biological food web that can support large macrofauna (Tebbs, Remedios, Avery, Rowland, and Harper (2015)) may suggest a less efficient carbon sink.

These high rates of primary productivity can be attributed to microbial mats. Cyanobacteria, eukaryotic algaes, and bacteria form facultative symbiont communities composed of layers defined by different taxa and metabolic requirements, and are linked through a diverse network of metabolites that cycle between the laminae. Microbial mats are one of the most ancient organisms on the planet and have been found as far back as 3.2 Ga in the sedimentary record (Noffke, Eriksson, Hazen, and Simpson

[0]**Abbreviations:** EtOH, ethanol; SEM, scanning electron microscope/microscopy

(2006)). Because microbial mats are mostly soft organic matter that does not fossilize, they are preserved in the rock record as microbialites. Microbialites do not contain the original organic matter of the microbial mat but instead contain carbonate muds that formed in conjunction with the resident microbes. They are associated with ancient paleolakes where high salinity was normally present and seasonal evaporation would render the lake completely dry (desiccation). Examples include microbialites from the west Qaidam Basin, China (Li et al. (2024)), the Green River Formation, U.S. (Eljalafi and Sarg (2021)), and the Madrid and Duero basins, Spain (Sanz-Montero and Rodríguez-Aranda (2022)). The three major forms of microbialites are typically determined by dominant cellular morphology, sedimentation method (i.e., precipitation vs. trapping and binding), and erosive fluid forces(Prieto-Barajas, Valencia-Cantero, and Santoyo (2018); Riding (2011); White (2020)), but regardless of the form, they are known to contain carbonate minerals that are historically difficult to precipitate out under low-temperature abiotic conditions (Arvidson (1999); Daye, Higgins, and Bosak (2019); Heim (2011); Land (1998)). It is therefore suspected that hard-to-form carbonates are biologically-mediated; hard-to-form carbonates found off the planet have been used to suggest the presence of extraterrestrial microbes (Nichols, Pontefract, Dion-Kirschner, Masterson, and Osburn (2023); Tutolo and Tosca (2023)).

Living microbial mats globally persist to this day, and they have become both an organism and ecosystem of interest to carbonate scientists. They are found in a myriad of environments, and those that inhabit alkaline lakes are specifically known as alkaliphilic microbial mats. In combination with the high DIC, pH, and alkalinity, previous studies looking into alkaline lake carbonate formation have found that many of the hard-to-form carbonates quite easily form in close proximity with these particular mats.

The Caribou Plateau in British Columbia hosts dozens of alkaline lakes, alkaliphilic microbial mats, and lacustrine carbonates (Raudsepp, Wilson, Zeyen, Arizaleta, and Power (2024)). Some lakes contain modern-day laminar microbialites that have been partially mineralized. In deeper alkaline lakes such as Pavilion Lake, mineralized microbialites are large and have diverse, depth-dependent morphologies (Schulze-Makuch et al. (2012)). They preserve their internal structure, yet in shallower lakes, harvested microbial mats show very poor lamination preservation, with evidence of sediment disturbance underneath the mats (Renaut and Long (1989)). This lack of preservation appears to inhibit effective carbonate mud formation when compared to more established colonies. However, they still have the potential for biologically-mediated carbonate formation.

In this study, we aim to identify individuals of local microbial mats to account for differences in distribution and microbial mat morphologies, along with attempts to assign metabolisms and further develop the alkaline lake chemical cycles. We also aim to present findings on alkaline lake surface and pore water chemistry and to apply them to saturation state models to predict what carbonates are forming in the Caribou Plateau lakes.

2 | METHODS AND MATERIALS

2.1 | Study Location

Goodenough Lake and Milk Lake are located in the Caribou Plateau, British Columbia approximately 26.7 km north of the village of Clinton and 17.2 km west of 70 Mile House (Fig. 1 a). The plateau is known ancestrally as Secwepemcúlecw to the Secwépemc First Nations, and ranges from 600 to 2000 m in elevation (Renaut and Long (1989)). During the last glacial period (115-11.7 ka), the Caribou Plateau was fully covered in ice and then exposed 10-9.5 ka (Renaut and Long (1989)), leaving a thick deposit of till that was later eroded by glacial melt. The modern-day topography is a direct result of deglaciation (Raudsepp et al. (2024)). Today, Goodenough and Milk Lake lie within the cold semi-arid climate (BSk) region of the Köppen climate classification and are within 5 km of the cold desert climate (BWk) (Peel, Finlayson, and Mcmahon (2007)). Geologically, they sit on top of the Chilcotin group flood basalts (Anderson et al. (2001); Bevier (1983)). Maximum annual precipitation is 400 mm, with most occurring in spring and summer. There is very little, if any, riverine fluxes to these lakes, resulting in hydrology that is majorly defined by groundwater, precipitation, and evaporation. At the time of the study, June had the highest precipitation on record at 53.4 mm total (Gov. of Canada, 2023) and the lakes were relatively deep and filled with surface and benthic algae. During the summer dry season, evaporation removes water and leaves Milk Lake and Goodenough Lake more saline, resulting in salt and carbonate precipitation along the lakeshore (Fig. 1 b).

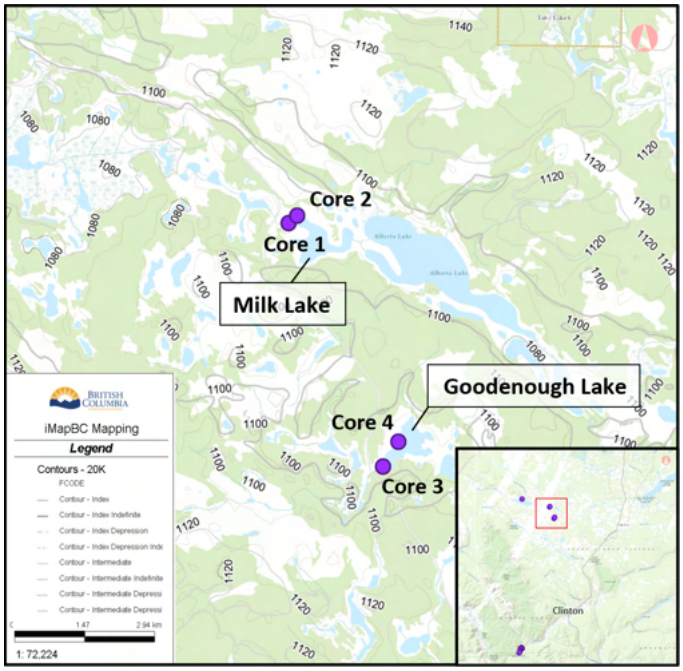

(a) Location of sampling area. General area lies approximately 35 km north of Clinton, British Columbia. Cores 1 and 2 were sampled from Milk Lake. Cores 3 and 4 were sampled from Goodenough Lake

(b) Goodenough Lake during the summer with carbonate ring along the lakeshore.

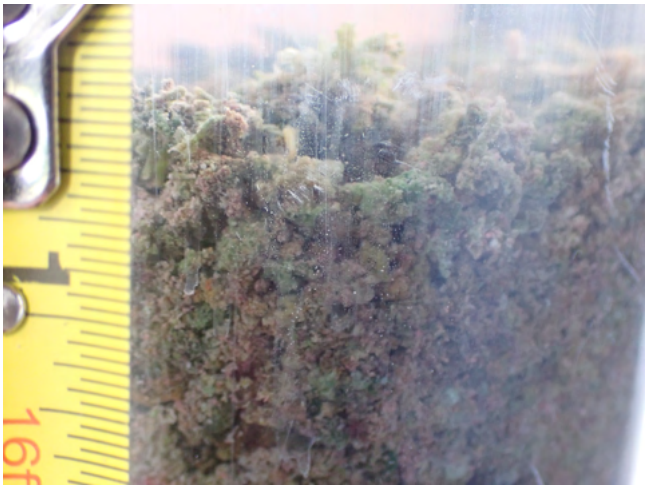

(c) Goodenough Lake sediment core showing green and purple microbe communities.

FIGURE 1 Field Site

2.2 | Sampling and Storage

Field sampling was conducted in late May and early June 2023. Across the two lakes, 56 samples were collected: 18 encrusted soil samples, 23 water samples, 11 microbial mat samples, and four sediment push cores. The encrusted soil samples were taken from the mud flats next to Milk Lake and Goodenough Lake, and were collected with a 50 mL Falcon tube as a 30 mm diameter 'push core' along a transect line at 1 to 2 m intervals. Four water samples were collected from Goodenough Lake and 19 samples from Milk Lake. These samples were collected from the lake surface in the shallow waters near the shore, and were filtered through a 0.22 μm syringe filter with a Nylon membrane. For each of the water samples, pH was measured in the field and again in lab with a Milkwaukee MW102 PRO+ meter on a total pH scale (calibrated prior to lab use with Indo pH 4.0 and

7.0 solutions). Microbial and algal mats were harvested from the surface of and at 2.5 cm depth at Goodenough Lake and Milk Lake with a trowel, and stored in 90% EtOH.

Sediment push cores from Milk Lake and Goodenough Lake (Fig. 1 c) were obtained with a 2 in diameter PVC core barrel, and pore fluid was extracted using 2.5 mm diameter rhizons with a mean pore size of 0.15 μm. While in the field, samples were stored in a cardboard box in the vehicle. On return to the University of Victoria, water and pore samples were stored at 4 °C while mat and encrusted soil samples were stored at room temperature in a cabinet.

2.3 | Microscopy

The surface of encrusted soil samples was scraped off with a scalpel onto a microscope slide and viewed through a Leica Wild M3Z vertical incident light stereomicroscope with a zoom magnification system of 6.5 to 40x. Small portions of mat samples were viewed in the same way, and additionally viewed through a Nikon ECLIPSE 80i light microscope with 10x and 20x objective magnification and a Nikon Microscope Y-IM Magnification Changer attachment with 1x, 1.25x, 1.5x, 2x magnification. Köhler illumination was used to enhance contrast and reduce image artifacts. Encrusted soil, mat, and precipitate experiment samples were prepared in various ways for scanning electron microscopy (SEM) and energy dispersive spectroscopy (EDS). Encrusted soil samples were kept under vacuum for 24 hours to remove remaining moisture and were not chemically fixed. Mat samples were fixed with four rounds of 2.5% glutaraldehyde soaking for five minutes. Precipitate experiment samples were left to completely dry in a fumehood for three days. All samples were then mounted on carbon sticky tape and carbon-coated (approx. 1.5 nm thickness) in a Cressington 208C sputter coater. Imaging was done at the University of Victoria's Advanced Microscopy Facility on a Hitachi S-4800 field emission scanning electron microscope at 5 kV. Elemental analysis was done with a Bruker Quantax EDS system at 10 kV.

2.4 | Dissolved Inorganic Carbon Analysis

Dissolved inorganic carbon (DIC) was measured with the UIC Model 5014 Coulometer and Standard Operating Procedure (SOP) protocols from Dickson, Chris, and Christian (2007). A fluorescence calibration curve was created using 2 ml, 4 ml, 6 ml, 8 ml, and 10 ml of certified seawater reference standard ([DIC] = 2012.0 μmol/kg), and was performed during coulometer start-up and before each sample run. 1 ml of 8.5% H_3PO_4 was added to 1 ml of sample to remove carbon. An internal reference was measured to check for reproducibility (Saanich Inlet seawater = 1599.6 ± 226.8 μmol/kg, 2σ, n = 8). Sample volumes were varied to ensure DIC measurements would fall within the calibration curve range.

2.5 | Alkalinity and Titration Analysis

Alkalinity was measured using Dickson & Sabine's (2007) manual titration technique and determined using the Gran Function Plot method from USGS's Alkalinty calculator. 10 ml of sample was diluted 5x with Milli-Q water. Prior to titration, pH was measured for the stock and 5x sample to account for pH change due to adding water. HCl (0.0927 μmolal) was slowly added to the stirring sample while volume and pH were recorded for every 0.5 increment of pH change. The sample was allowed to stabilize after each amount of acid was added. Initial pH ranged from 9.2-10.4 for Goodenough Lake and 9.8-10.2 for Milk Lake. Generally, each sample was titrated to a pH of 3.0. Between carbonate points (pH 7.0, 4.0, and 3.5-3.0), the volume of acid added was recorded for every 0.1 increment of pH change for better accuracy when using the Gran Function plot to calculate alkalinity. Uncertainty was measured using the 5 duplicate samples ($2\sigma = 0.824$ meq/kg).

2.6 | Ion Chromatography

For ion analyses, liquid samples were diluted appropriately with MilliQ water and measured using a Thermo Scientific Dionex ICS-6000 high-pressure ion chromatographer (HPIC). Anions (F^-, Br^-, Cl^-, NO_2^-, NO_3^-, CO_3^{2-}, SO_4^{2-}, PO_4^{3-}) were measured with a multi-step gradient method starting from 4.70 mM of KOH to 28.00 mM. Column temperature was kept 30.00 °C while compartment temperature was kept at 15.00 °C. Cations (Li^+, Na^+, NH_4^+, K^+, Mg^{2+}, Ca^{2+}) were measured with an isocratic method at a concentration of 25 mM MSA. Column temperature was kept at 40.00 °C while compartment temperature was kept at 20.00 °C.

2.7 | Precipitation Experiment

To investigate the effect of storing mat samples in EtOH, precipitate experiments were performed using mixed 'stocks' from surface water samples. Two different experiments were designed (Table 1), each with a sub-experiment investigating the effect of different mineral nucleation seeds; calcite ($\leq$50 μm particle size, M = 100.09 g/mol) (Pan et al. (2021)) versus kaolinite (M = 258.16 g/mol) (Molnár, Pekker, Dódony, and Pósfai (2021)). Experiment 1 consisted of precipitation in a mix of sample stock and 90% EtOH. Experiment 2 consisted of precipitation in a mix of samples stock spiked with Ca. A control experiment was also performed for each mineral nucleation seed. Each experiment consisted of 10 mL of Milk or Goodenough stock with 30 mg of each nucleation seed. For experiment 1, 40 mL of 90% EtOH was added, while for experiment 2, 93.5 μL of 10K ppm Ca to the Ca-specific vials, targeting an approximate Mg/Ca ratio of 1 mol/mol of the final solution. All samples were capped and placed at an angle on a Heildolph Unimax 1010 shake table at 69 rpm. Once a week, approximately 0.7 mL of sample fluid was filtered through 0.22 μm, appropriately diluted with MilliQ water, and analyzed with the Dionex ICS-6000 HPIC for cation concentrations. After six weeks, the samples were spun down in a Sorvall Legend RT at 2000 rpm for 20 minutes. Samples were decanted, and the remaining pellets were left to dry in a fumehood for three days. Pellets were then carbon coated and imaged on the SEM.

	Stock (10 mL)	Seed and Weight (g)	Ethanol (40 mL)	Ca Spike?	Replicate for…
Exp 2, Sample 1	Milk	Kaolinite - .0322	No	No	-
Exp 1, Sample 2	Milk	Kaolinite - .0298	Yes	No	-
Exp 2, Sample 3	Milk	Kaolinite - .0312	No	Yes	-
Exp 2, Sample 4	Milk	Kaolinite - .0317	No	No	Sample 1
Exp 1, Sample 5	Milk	Kaolinite - .0328	Yes	No	Sample 2
Exp 2, Sample 6	Milk	Kaolinite - .0326	No	Yes	Sample 3
Exp 2, Sample 7	Milk	Calcite - .0290	No	No	-
Exp 1, Sample 8	Milk	Calcite - .0288	Yes	No	-
Exp 2, Sample 9	Milk	Calcite - .0297	No	Yes	-
Exp 2, Sample 10	Milk	Calcite - .0290	No	No	Sample 7
Exp 1, Sample 11	Milk	Calcite - .0288	Yes	No	Sample 8
Exp 2, Sample 12	Milk	Calcite - .0297	No	Yes	Sample 9
Exp 2, Sample 13	Goodenough	Kaolinite - .0296	No	No	-
Exp 1, Sample 14	Goodenough	Kaolinite - .0328	Yes	No	-
Exp 2, Sample 15	Goodenough	Kaolinite - .0320	No	Yes	-
Exp 2, Sample 16	Goodenough	Kaolinite - .0303	No	No	Sample 13
Exp 1, Sample 17	Goodenough	Kaolinite -.0320	Yes	No	Sample 14
Exp 2, Sample 18	Goodenough	Kaolinite - .0327	No	Yes	Sample 15

TABLE 1 Qualities of each sample in precipitation experiment

2.8 | Evaporation and Mineral Precipitation modeling

To investigate the controls on the geochemistry of water samples from Goodenough and Milk Lake, models were developed using the Phase and React tools of the Geochemist's Workbench (GWB v.17.0.2). Initial ion conditions for the model were determined by taking the average of ion concentrations from the three lowest [Na^+] and [ALK] Milk Lake surface water samples to represent the least evaporated samples. The initial water mass was set to 50 g, as ion concentrations were measured from the 50 mL Falcon tubes. The user-defined reaction continuously removed 1 g H_2O/day from the system for 49.9 in-model days. Both the initial and final states of the system were viewed and compared to the cation and anion concentrations of water samples, in addition to the X-Ray fluorescence (XRF) reports generated from the Bruker Quantax EDS.

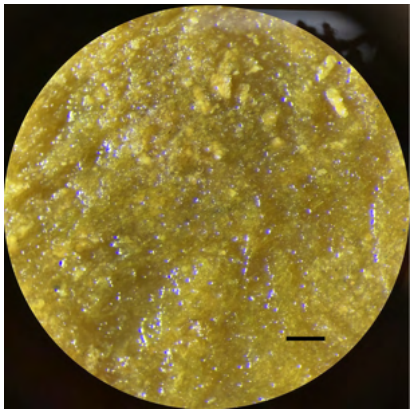

(a) Milk Lake surface mat.

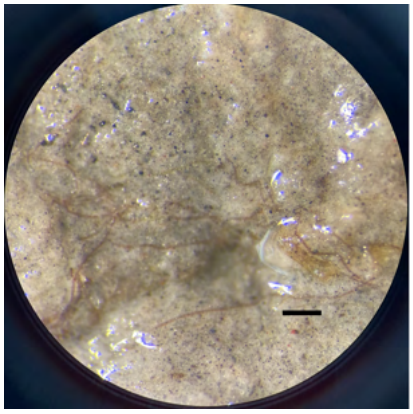

(b) Milk Lake benthic mat showing sparse abundance of algal strands.

(c) Goodenough Lake mat micrograph showing well consolidated mats with nodules underneath organics.

FIGURE 2 Lake mat micrographs. Taken through a Leica Wild M3Z. 40x total magnification. Scale bars, 0.5 mm

3 | RESULTS

3.1 | Microbial Community Morphology and Composition

Milk Lake has two distinct mats that grow on the water surface and on the lake bed. The morphology of the surface growing mat is uniform and is composed of long colonial algae residing in segmented cell walls. White 0.25-0.5 mm long sediments are seen under the surface of the mat (Fig. 2 a). Benthic mats appear to have the same algae but in much less abundance (Fig. 2 b). The algal strands are too sparse to bind sediments or serve as an efficient locus for mineral precipitation. Mats from Goodenough Lake are more tightly bound together and have rounded carbonate nodules that lie underneath, giving the surface a texture best summarized as "fried chicken" (Fig. 2 c).

The cellular morphology of the mats from the two lakes differs greatly. Goodenough Lake cells are typically 3-5 μm in width with large variations in length ($\geq$ 100 μm) (Fig. 3 a). The dominant morphologies are Spirulina and Oscillatoria-like and are tightly wound with each other, along with Synechococcus-like cells in much smaller abundance (Fig. 3 b). The dominant color is green-brown, with occasional red unicellular organisms appearing. Filamentous cells are thoroughly knotted within each other and form chunks ranging from 75 μm to 300< μm in diameter (Fig. 3 a and 3 b). Mineral nodules of varying sizes appear near or on the surface of cell walls (Fig. 3 c). The most abundant cells in Milk Lake are much larger, being 30 μm wide and a few centimeters long (Fig. 2 a and 3 d). These cells appear structurally similar to some members of the Spirogyra genus; Figure 3 f shows conjugation tubes between strands and zygotic cells specific to the taxon (Yoou, Kim, and Kim (2009)). Oscillatoria-like and heterocystic cells are seldom found between them. Between Goodenough Lake and Milk Lake, encrusted soil samples appear similar, although Goodenough Lake samples sport greater color variation. Milk Lake soil samples more commonly had grass in them.

3.2 | Surface Water

3.2.1 | Salinity

Evaporation trends between lakes are compared by plotting salinity against Na^+ and against alkalinity (Fig. 4). Milk Lake and Goodenough Lake follow a similar linear trend ($R^2_{Na} = 0.9987$, $R^2_{Alk} = 0.9975$), with Goodenough Lake showing a higher concentration of salinity likely due to greater evaporation. As a result, Goodenough Lake salinity and ion concentrations were higher than Milk Lake. To better compare their relative concentrations and trends, ion, alkalinity, and DIC concentrations for field samples are normalized to Na^+ to set a common scale.

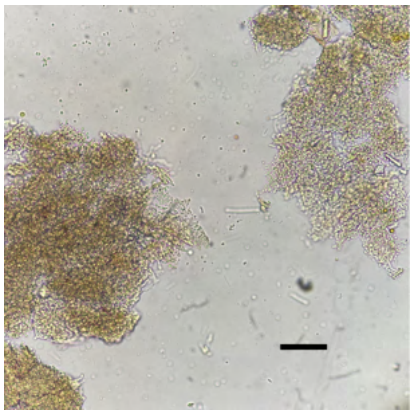

(a) Goodenough Lake mat showing cell chunks. Scale bar, 50 μm.

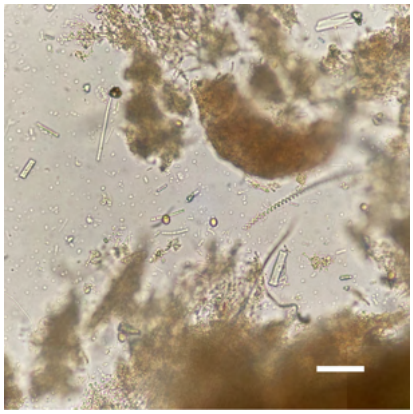

(b) Spirulina-shaped cell and rectangular minerals from Goodenough Lake mat. Scale bar, 50 μm.

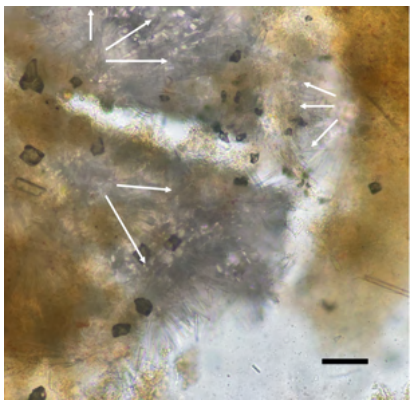

(c) Goodenough Lake mat with radiating in situ crystals. Arrows point away from locus. 400x magnification. Scale bar, 50 μm.

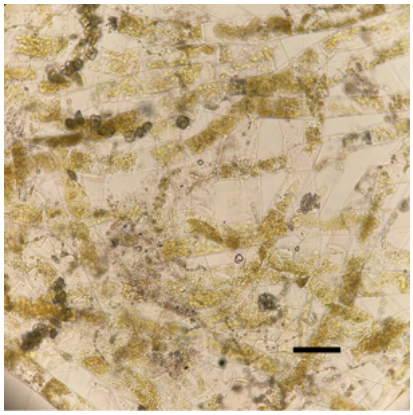

(d) Milk lake mat colonial algae with multi-segmented sheath and lysed cell contents. Heterocystic cells in background. 200x magnification. Scale bar, 100 μm.

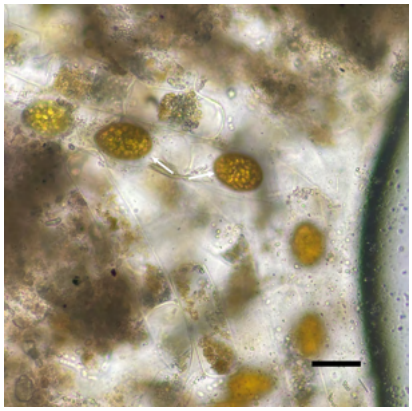

(e) Milk lake mat colonial algae with intact cells. Radiating minerals appear to grow from within cell wall. 400x magnification. Scale bar, 50 μm.

(f) Biological structures of cell and cell wall suggests sample belongs to the Spirogyra genus. 400x magnification. Scale bar, 50 μm.

FIGURE 3 Goodenough Lake and Milk Lake mat micrographs. Taken through a Nikon 80i Eclipse.

3.2.2 | Alkalinity and DIC

DIC shows little significant difference between Milk and Goodenough Lake. Due to the normalizing to Na^+ (mmol/L), the reported DIC concentrations are unitless assuming 1 L H_2O is equal to 1 kg H_2O. Milk Lake ranges from 3.18e-4 $\pm$ 0.00188 to 0.800 $\pm$ 0.00431, although most samples gather around concentrations between 0.530 $\pm$ 0.00260 and 0.800 $\pm$ 0.00431 (2σ, N = 19). Goodenough Lake ranges from 0.483 $\pm$ 0.00083 to 0.673 $\pm$ 0.00080 with an outlier at 1.42 $\pm$ 0.01040 (not plotted) (2σ, N = 4). Alkalinity shows a greater difference between the surface of the lakes. Milk Lake is overall higher and ranges from 0.979 $\pm$ 0.00675 meq/mmol to 1.08 $\pm$ 0.01473 meq/mmol. An outlier of 10.7 $\pm$ 0.0123 meq/mmol is not plotted (2σ, N = 19). Goodenough Lake ranges from 0.892 $\pm$ 0.00296 meq/mmol to 0.912 $\pm$ 0.00304 meq/mmol with an outlier at 1.24 $\pm$ 0.03932 meq/mmol (2σ, N = 4).

3.2.3 | Lake surface water cation and anion concentrations

The cation and anion concentrations in Goodenough and Milk Lake show variable differences that range from not significant to greatly significant. Goodenough Lake is not significantly higher in normalized ammonium ($[NH_4^+]_{max}$ = 1.16 $\pm$ 0.138 μmol/mmol, 2σ, N = 4) in comparison to Milk Lake ($[NH_4^+]_{max}$ = 0.51 $\pm$ 0.631 μmol/mmol 2σ, N = 19), although there is a Goodenough outlier with a concentration of 10.46 $\pm$ 1.84 μmol/mmol and a Milk outlier with a concentration of 2.22 $\pm$ 0.580 μmol/mmol. However, Goodenough Lake is significantly greater in normalized sulfate than Milk Lake ($[SO_4^{2-}]_{Good.max.}$ = 0.162

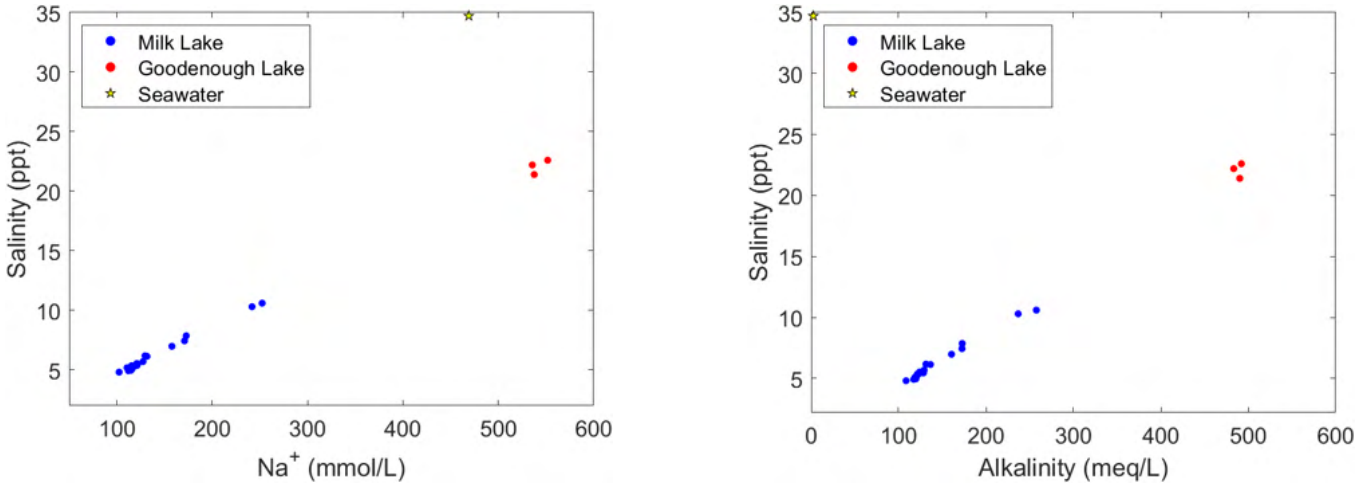

(a) Lake surface and seawater salinity against surface Na^+. $R^2 = 0.9988$

(b) Lake surface and seawater salinity against surface alkalinity. $R^2 = 0.9975$

FIGURE 4 Seawater values from Toggweiler and Sarmiento (2013)

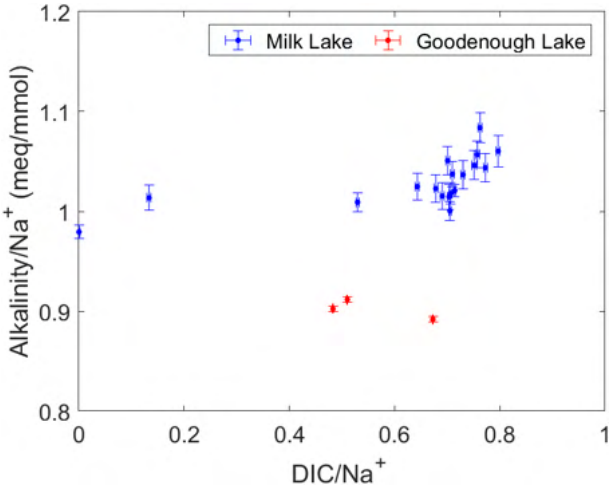

FIGURE 5 Alkalinity against DIC (outliers omitted)

$\pm$ 2.71x10^{-5}, 2σ, N = 4; $SO_4^{2-}]_{Milkmax.}$ = 0.0275 $\pm$ 7.11x10^{-5}, 2σ, N = 19) (Fig. 6). Goodenough Lake also had a noticeable sulfuric smell while collecting samples, indicating the presence of H_2S and suggesting microbial SO_4^{2-} reduction.

When comparing Ca^{2+} and Mg^{2+}, the maximum concentrations in Goodenough lake are 0.168 $\pm$ 0.00831 μmol/mmol and 3.75 $\pm$ 0.0452 μmol/mmol respectively ($[Ca^{2+}]_{Good.outlier}$ = 1.24 $\pm$ 0.107 μmol/mmol, 2σ, N = 4; $[Mg^{2+}]_{Good.outlier}$ = 120.0 $\pm$ 0.538 μmol/mmol, 2σ), and are both significantly lower than Milk Lake maximums ($[Ca^{2+}]_{Milkmax.}$ = 0.566 $\pm$ 0.0387 μmol/mmol, 2σ, N = 19; $[Mg^{2+}]_{Milkmax.}$ = 25.1 $\pm$ 0.233 μmol/mmol, 2σ, N = 19; $[Ca^{2+}]_{Milkoutlier}$ = 1.04 $\pm$ 0.0338 μmol/mmol) (Fig. 6 b). The low Ca^{2+} concentrations in both lakes make the magnitude of Mg^{2+} changes appear greater between lakes (Fig. 6 b).

3.3 | Core Pore Fluid Ion Profiles

The depth profiles from the sediment core pore-fluid samples show significant difference between sodium concentrations in Goodenough and Milk Lakes. All reported errors are 2σ from the average precision of the chromatographer standards. Milk Lake shows a small but steady Na^+ increase with depth in both cores, with a maximum of 202 $\pm$ 0.0166 mmol/L (2σ) at 13 cm in the red core (Fig. 7). Goodenough Lake shows a much greater concentration of sodium at the top of the core. The

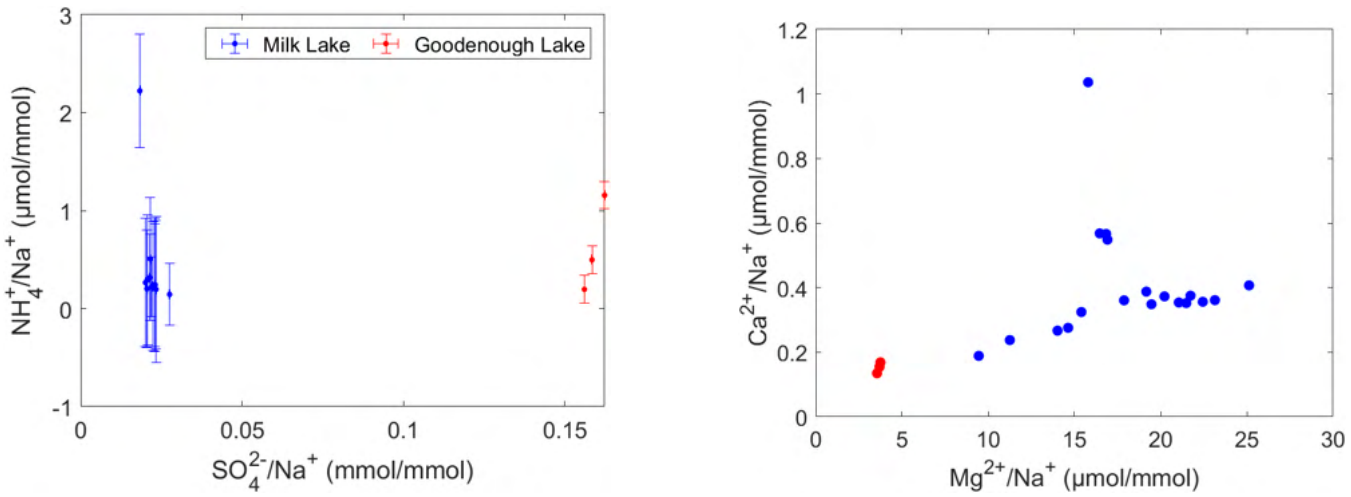

(a) NH_4^+ against SO_4^{2-}.

(b) Ca^{2+} against Mg^{2+}, normalized to Na^+

FIGURE 6 Anion Comparisons between Goodenough Lake and Milk Lake surface water samples. Error bars represent 2σ from calibration curve mean.

purple Goodenough core initially decreases with depth ($[Na^+]_{min.} = 492 \pm 0.0166$ mmol/L at 6 cm, 2σ) before increasing to a maximum of 642 ± 0.0166 mmol/L at 16 cm (2σ). The orange core trends similarly with purple core before breaking down and sporadically changing at 8 cm (Fig. 7). When normalized to Na^+, NH_4^+ concentrations show similar trends between all cores, but the magnitude of change in the Goodenough Lake cores is four to five times greater (max $[NH_4^+]_{norm.} = 19.8 \pm 0.148$ μmol/mmol at 8 cm_{purple}, 2σ) than observed in the Milk Lake cores (max $[NH_4^+]_{norm.} = 3.14 \pm 0.550$ μmol/mmol at 4 cm_{red}, 2σ). Measured Mg^{2+} concentrations in core pore-fluid show small and consistent changes with depth. In Milk Lake, the initial concentration at the sediment-water interface ($[Mg^{2+}]_{norm.} = 8.90 \pm 0.178$ μmol/mmol at 0 cm_{red}, 2σ; $Mg^{2+}{}_{norm.} = 2.08 \pm 0.238$ μmol/mmol at 0 cm_{blue}, 2σ) rapidly decreases before stagnating between 5-10 cm and then increasing slowly ($Mg^{2+}{}_{norm.} = 1.08 \pm 0.141$ μmol/mmol at 17 cm_{red}, 2σ; $Mg^{2+}{}_{norm.} = 2.07 \pm 0.149$ μmol/mmol at 15 cm_{blue}, 2σ) In Goodenough Lake, the concentration at the top of the core is the maximum, as Mg^{2+} decreases with depth.

3.4 | Goodenough Encrusted Soil Elemental Composition with EDS

Goodenough Lake encrusted soil samples were analyzed on the SEM with EDS, and show spatially varied elemental distribution. In appendix Figure B7 , silica and aluminum overlap consistently with each other and show a light even spread with heavier distribution on the left side. The spectrum suggests that Si is found in 5x abundance relative to Al. Na appears to overlap with Si and Al but not to the same extent. Its abundance appears similar to Al. Ca and Mg have spatially similar abundances along the top portion of the micrograph; Ca appears to extend further down. It also shows more grouping than Mg, suggesting a sporadic distribution of Ca-mineral hotspots. The spectrum indicates that Mg is in much greater abundance, and is the most abundant element after O.

3.5 | Precipitate Experiments

IC chromatography and pH measurements were done on filtered sample fluid weekly for six weeks; Figures 9 and D8 show the changes in cations and pH over time. For measurements done on December 15, there appear to be sudden dips or peaks that are not reflected in technical replicates, suggesting a possible error in cation analysis. However, because initial and final conditions typically fall within 2σ of each other, we can be confident in those values.

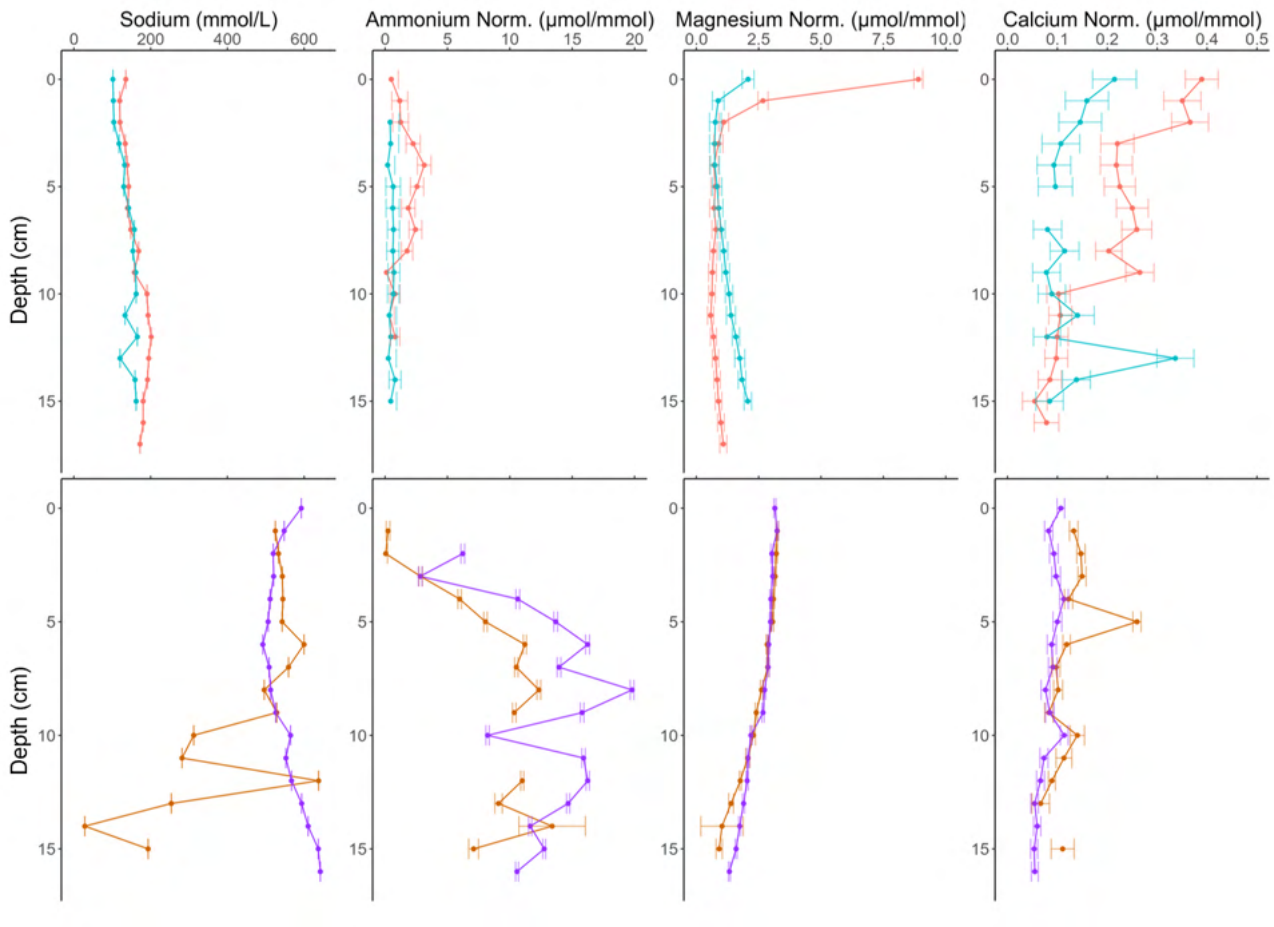

FIGURE 7 Depth profile of normalized cation concentrations from push core pore-fluid. Blue, Red: Milk Lake cores. Orange, Purple: Goodenough Lake cores.

FIGURE 8 Crystals forming in Goodenough-kaolinite sample an hour after EtOH addition.

3.5.1 | Ca Spiked Samples

Ca-spiked samples contained 0.926% 10K ppm Ca solution and 99.1% lake water and were meant to serve as a simulation for how soluble ions change and what minerals precipitate from solution when a Ca influx is introduced (Deutsch, Jenne, and Krupka (1982)).

Cation concentrations

In Figure 9 b, the final Na^+ concentrations for Milk stock samples were relatively unchanged throughout the experiment, and show a very small decrease by the end (average $\Delta[Na^+]_{Milk.}$ = -4.09 ± 0.0166 mmol/L, 2σ, N = 4). Both Goodenough Lake samples have a net loss of Na^+ by the end of the experiment. (average $\Delta[Na^+]_{Good.}$ = -52.1 ± 0.0166 mmol/L, 2σ, N = 2). Na^+ is the only cation that differentiates between lake stock water. Measured NH_4^+ shows variation between technical replicates, however more extreme values still fall outside of the 2σ range of cation analysis precision. For almost all samples, NH_4^+ is higher by the end of the experiment ($\Delta[NH_4^+]_{average}$ = 3.63 ± 3.95 μmol/L, 2σ, N = 5, calcite Milk outlier omitted) (Fig. 9 e). Ca^{2+} shows a sharp decrease from the initial concentration ($[Ca^{2+}]_{init.average}$ = 410 ± 1.53 μmol/L, 2σ, N = 6) before stabilizing at a lower concentration. Although some variation occurs on samples that were analyzed on December 15, they later converge on the final day of analysis ($[Ca^{2+}]_{averagefin.}$ = 75.1 ± 1.35 μmol/L, 2σ, N = 6) (Fig. 9 h). Mg^{2+} stays fairly consistent throughout the experiment, with only a small decrease by the final day ($\Delta[Mg^{2+}]_{average}$ = -0.289 ± 0.115 mmol/L, 2σ, N = 6) (Fig. 9 k). K^+ shows a net increase after six weeks ($\Delta[K^+]_{average}$ = .992 ± 0.0256 mmol/L, 2σ, N = 6) (Fig. 9 n). It is the second greatest change in cation concentration after Na^+

EDS Analysis

After six weeks of chromatography analysis, the seed pellets were spun down, dried for three days, and imaged on the SEM.

Figure D9 a shows bright minerals growing along the top of the flat kaolinite flakes from a Goodenough-kaolinite sample. These minerals range from 2-3 μm across, and appear to have a intersecting tabular habit (Klein and Philpotts (2016)). The brightness is partially indicative of a higher atomic weight than that of the surrounding kaolinite environment (Figs. D9 c, and D9 d)(Engel (1978)). Elements detected by the Bruker EDS Figure are layered over the micrograph and shown in Figure D9 k. Ca, Mg, Na, and K (Figs. D9 f, D9 h,D9 g, and D9 i) appear to show up as hotspots instead of an even dispersion like that of Fe (Fig. D9 j). These hotspots also overlap with one of the brighter surface minerals, with Ca and K having a higher concentration relative to Na and Mg overall (Fig. D9 b. Both Al and Si are high due to the presence of the kaolinite seed.

In a Milk-kaolinite sample, Figure D13 a shows similar brighter nodules, but not as brightly as in D9 a. We also find that many of the elements that are hotspotting do not necessarily overlap with the bright nodules (Fig D13 j). Ca forms extremely neat hotspots that Mg occasionally overlaps with (Figs. D13 f, and D13 g). In this sample, Mg and Na (Fig. D13 h) are more evenly spread across the micrograph with some hotspotting. K does not cluster in the same areas as Ca and Mg, but can be seen in a higher concentration on the bottom-left corner (Fig D13 i). A higher concentration of Si in Figure D13 d is seen aligning to the same K cluster. This sample has a similar spectrum to the Goodenough-kaolinite sample, showing a slightly greater amount of Ca than Na and Mg. K is, however, lower in this sample (Fig D13 b).

3.5.2 | EtOH Samples

EtOH samples contained 72% EtOH and 20% lake water. Within an hour of adding EtOH to the lake water and seed, we observed crystals precipitating out of solution (Fig. 8).

Cation Concentrations

Cation concentrations from EtOH samples are extremely variable, and odd trends appear when plotted as a time series (Fig. 9).

In Figure 9 c, the initial and final Na^+ concentrations for Milk-calcite samples do not overlap ($[Na^+]_{Calcite.init.replicate.1}$ = 14.5 ± 0.0166 mmol/L, 2σ, N = 1; $[Na^+]_{Calcite.init.replicate.2}$ = 17.8 ± 0.0166 mmol/L, 2σ, N = 1; $[Na^+]_{Calcite.fin.replicate.1}$ = 14.6 ± 0.0166 mmol/L, 2σ, N = 1; $[Na^+]_{Calcite.fin.replicate.2}$ = 20.2 ± 0.0166 mmol/L, 2σ, N = 1). The increase in Na^+ is not odd, as there is no additional source of Na^+ being added over time. In kaolinite samples, Goodenough Lake water samples begin at approximately the same concentration, but do not end on the same concentration. Milk Lake water samples are also varied. With the exception of one Milk Lake sample, all kaolinite samples show a net decrease in Na^+.

Figure 9 f shows two sets of NH_4^+ trends. In both calcite samples and one Milk-kaolinite sample, a sharp spike is seen on December 15 which likely correlates with unexpected cation deviations on that day. For the remaining kaolinite samples, NH_4^+

is ranges from 19.8 to 77.9 ± 15.8 μmol/L (2σ) throughout the time series. All samples converge around the same approximate concentration ($[NH_4^+]_{fin.average}$ = 52.0 ± 15.8 μmol/L, 2σ, N = 6; $[NH_4^+]_{fin.maximum}$ = 77.9 ± 15.8 μmol/L, 2σ, N = 6; $[NH_4^+]_{fin.minimum}$ = 21.2 ± 15.8μmol/L, 2σ, N = 2).

Ca^{2+} follows a similar trend to NH_4^+ for all samples, however both Milk-kaolinite samples peak at December 15. The final concentration ranges from 13.4 to 38.6 ± 1.35 μmol/L (Fig. 9 i)

Mg^{2+} also follows a similar trend to NH_4^+ and Ca^{2+}, especially in Milk Lake samples (Fig. 9 l). Goodenough Mg^{2+} does not extend to the last day, as it was no longer at detectable levels.

K^+ increases consistently in the Milk-calcite samples before plateauing around 1.5 ± 0.119 mmol/L (2σ, N = 4). In all kaolinite samples, there is no discernible trend. Goodenough-kaolinite samples start near the same initial concentration ($[K^+]_{average.init.}$ = 0.528 ± 0.00271 mmol/L, 2σ, N = 2) and end at significantly different concentrations (Fig. 9 o). Milk-kaolinite samples start at significantly different concentrations, and end on nearly the same final concentrations ($[K^+]_{averagefin.}$ = 1.42 ± 0.31 mmol/L, 2σ, N = 2).

EDS Analysis

EtOH samples appeared to be the most reactive, and caused a large decrease in soluble cations when compared to the Ca-spiked and control samples (Fig. 9), leading to the formation of minerals with unique crystal habits (Stoica et al. (2004)).

When analyzing the crystals grown from a Goodenough-kaolinite sample, a prismatic radiating aggregate (Klein and Philpotts (2016)) with individual crystal lengths >100 μm (Fig. D11 a) is present. According to the elemental maps, these crystals are majorly composed of Na (Fig. D11 h) with small clusters of Mg and K either in or under the crystals (Figs. D11 i, and D11 g). In the spectrum, Na abundance all but dominates; the peak is so large that it partially envelopes the Mg and Al peaks. Around 2.3 an unmarked peak appears, and around 3.3 keV, we see a small K peak (Fig. D11 b).

Crystals grown from a Milk-calcite sample grow in a wave-pattern, and individual crystals appear approximately 5-10 μm long. The habit appears to be a combination of bladed and unidirectional radiating (Klein and Philpotts (2016)). The waving crystals appear to be composed of Si, Na, and Al (Figs. D12 d, D12 h, and D12 c). Mg and Ca clusters spatially coincide with each, but are not spatially associated with the Si-Na-Al crystals. Instead, Mg-Ca clusters grow in close approximation or within them (Figs. D12 g, and D12 f). Additionally, S appears in the EDS analysis, and overlaps with some K clusters. These clusters do not overlap with the Mg-Ca clusters or the Si-Na-Al crystals (Figs. D12 i, and D12 j). The spectrum shows a high Na abundance with lower but detectable abundances of S, K, and Ca. Mg has the smallest peak and is barely detectable (Fig. D12 b).

Crystals grown from a Milk-kaolinite sample are arguably the most visually interesting. The most discernible habit is the radiating acicular aggregate. They stand at a approximately 100 μm diameter. Individual needles have a width range from 2 μm to 5 μm. This is the only EtOH sample where Ca is not detected by the EDS system; instead the Mg is spatially associated with Na in the acicular crystals (Figs. D15 f, D15 g). Na is not only relegated to the crystals, and is found in clusters overlapping with S (Fig. D15 i)and Al (Fig. D15 c.) The spectrum is shown in Figure D15 b suggests that Na abundance is significantly higher, and only lower than Al and S. The Mg peak is also high, and is the highest when compared to Mg peaks from other EDS spectrums. The appearance of S is also interesting, as it was not recognized in other samples by the EDS system.

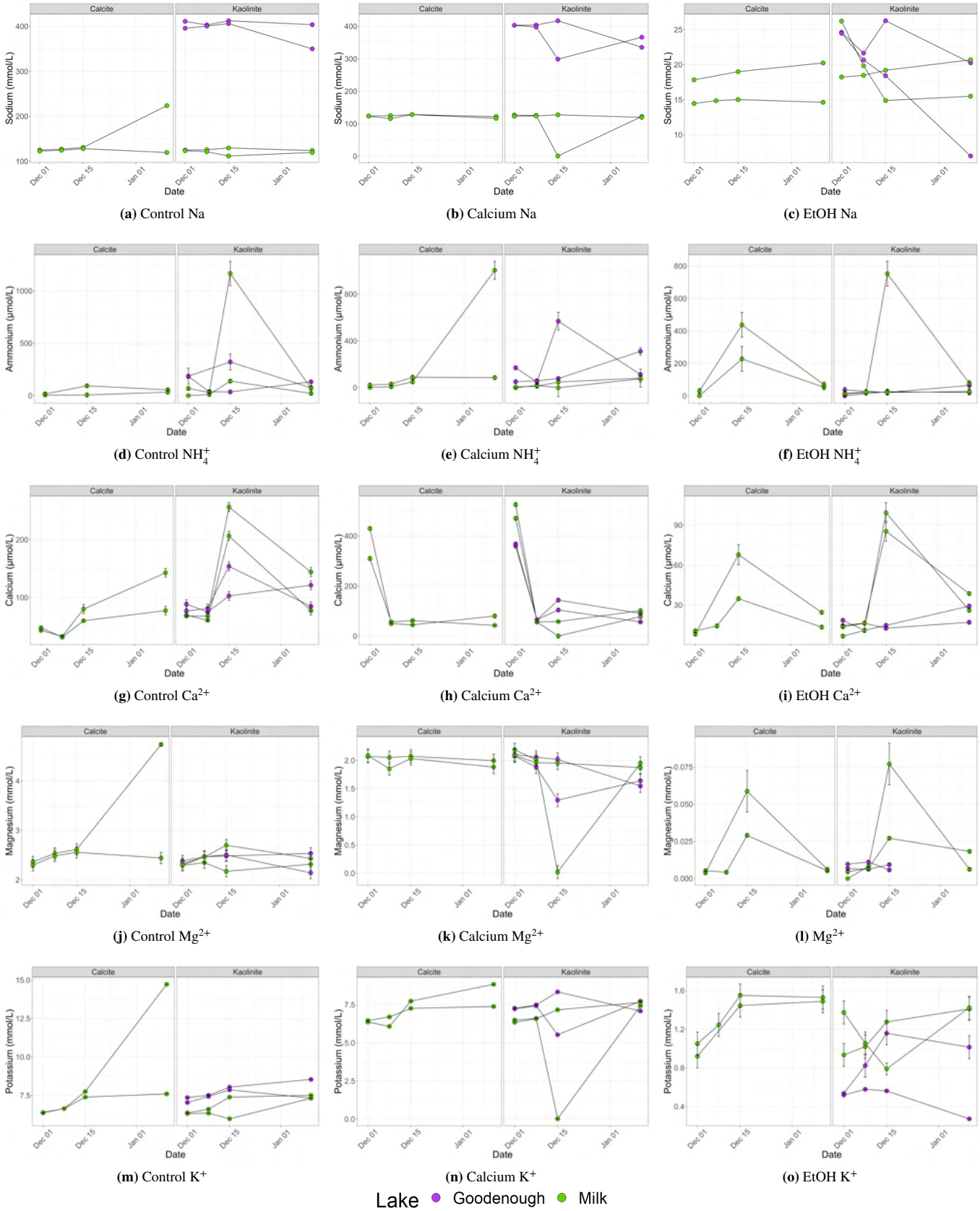

(a) Control Na **(b)** Calcium Na **(c)** EtOH Na

(d) Control NH_4^+ **(e)** Calcium NH_4^+ **(f)** EtOH NH_4^+

(g) Control Ca^{2+} **(h)** Calcium Ca^{2+} **(i)** EtOH Ca^{2+}

(j) Control Mg^{2+} **(k)** Calcium Mg^{2+} **(l)** Mg^{2+}

(m) Control K^+ **(n)** Calcium K^+ **(o)** EtOH K^+

FIGURE 9 Cation concentration time series separated by seed. Error bars represent 2σ from the average precision of the chromatographer's standard

4 | DISCUSSION

4.1 | Evaporation and Mineral Precipitation

The removal of H_2O from an undersaturated solution leads to an increase in analyte concentration relative to the overall mass or volume of H_2O (Tutolo and Tosca (2023)). A consequence of this higher concentration is the increase of a mineral's saturation index Ω (Keul, Morse, Wanninkhof, Gledhill, and Bianchi (2010)).

$$\Omega_{mineral} = \frac{[Cation][Anion]}{K^*_{mineral}}$$

where $K^*_{mineral}$ is the stoichiometric solubility product of the mineral. When Ω is < 1, a mineral is undersaturated and will not precipitate out of solution. Once the anion or cation concentration increases to $\Omega > 1$, the mineral is supersaturated and will precipitate out of solution until $\Omega < 1$ again.

When plotting for evaporation (Fig. 4), the trend strongly suggests that Milk Lake evolves to become chemically similar to Goodenough Lake once enough H_2O is removed. By taking evaporation into consideration, we can use it to explain significant differences in lake analytes. To further test this consideration on the evaporative transition, simple modeling was done with Geochemist's Workbench's (v17.0.2) React tool. Initial concentrations were defined in the model based on the lowest sodium and alkalinity concentrations observed in surface water samples (MILK8, MILK9, and MILK11) (Table C2 , Table C1).

In Figure 5 , Goodenough was found to have a slightly significant decrease in normalized DIC and alkalinity, although one point does overlap with the main Milk Lake sample cluster on the DIC axis. In our model, Figures E15 e and E15 g show Goodenough Lake increasing in both DIC (in HCO_3^- form) and alkalinity, but not at as fast of a rate as the Na^+ increase. With normalization in mind, this trend suggests a mechanism for DIC removal that sees a slight increase from 1.47 ALK:DIC average normalized Milk Lake ratio to 1.66 ALK:DIC average normalized Goodenough Lake ratio. Zeebe and Wolf-Gladrow (2001) simplify processes that affect DIC and total alkalinity in Figure 1.1.3. Goodenough Lake's decreasing in both alkalinity and DIC at a higher ratio suggests that carbonate formation is becoming a more dominant force for DIC and carbonate removal. We can now assume that Goodenough Lake does reach a state of supersaturation and decreases in DIC and alkalinity due to carbonate formation. Interestingly, the expected change in alkalinity and DIC is not represented when lake pH is taken into consideration. Figure 1.1.3 (Zeebe and Wolf-Gladrow (2001)) shows that carbonate formation results in a pH decrease of the solvent, and the evaporative model also corroborates this. But when plotting measured pH on the model, it appears that pH is actually increasing with evaporation E15 f. In Goodenough Lake and Milk Lake, it appears that there is an additional force that is strong enough to change pH and influence the rate of change in alkalinity and DIC. While we could attribute this to the release of aqueous CO_2, the high pH means that there is effectively none left in solution (Fig. 1.1.2Zeebe and Wolf-Gladrow (2001)). Instead, we can attribute this to high levels of photosynthesis (Haines, Khot, and Strous (2023); Zorz et al. (2019)), which still decreases DIC while only slightly increasing alkalinity.

We have discerned that carbonates are precipitating out of solution in Goodenough Lake at least, and our model corroborates this (Figs. 10 a and 10 b). Therefore, we should expect chemical analytes to follow our modeling trends. Most do follow with some variation; in Figure E16 d, Goodenough Lake lies below the expected $[K^+]$ value of 25 mmol/L ($[K^+]_{Good.average} = 9.76 \pm 0.951$ mmol/L, 2σ, N = 3), and in Figure E16 c, Goodenough lies above the expected $[SO_4^{2-}]$ value of 15 mmol/L with the exception of one outlier that was later rerun ($[SO_4^{2-}]_{Good.average} = 86.1 \pm 0.00163$ mmol/L, 2σ, N = 3).

The greatest deviations from the model were Ca^{2+} and Mg^{2+}, which were grossly underestimated (Figs. E16 a and E16 b. The model predicts that Mg- and Ca-carbonates precipitate out of solution instantly, which explains the initial low concentration. However, no precipitation occurred in our water samples, implying we are instead undersaturated in carbonate-forming constituents. That being said, we suspect the model is calculating a $K^*_{carbonate}$ value that is not perfectly reflective of the true lake environments (i.e., microbial kinetics (Brady, Druschel, Leoni, Lim, and Slater (2013)), rate of groundwater influx, variable water temperature), and is overpredicting $\Omega_{carbonate}$.

The model should not be fully disregarded, however, as there have been previous studies showing that predicted minerals were found in the field along the lakeshore (Raudsepp et al. (2024); Renaut and Long (1989); Tutolo and Tosca (2018)).

4.2 | *in situ* Biochemical Processes in Lake sediments

We should not discount the importance of *in situ* biochemical forces within lake bed sediments. Within sediments, oxygen becomes a major driver for metabolic processes; this is similarly seen in deep seawater columns (Emerson and Hamme (2022));

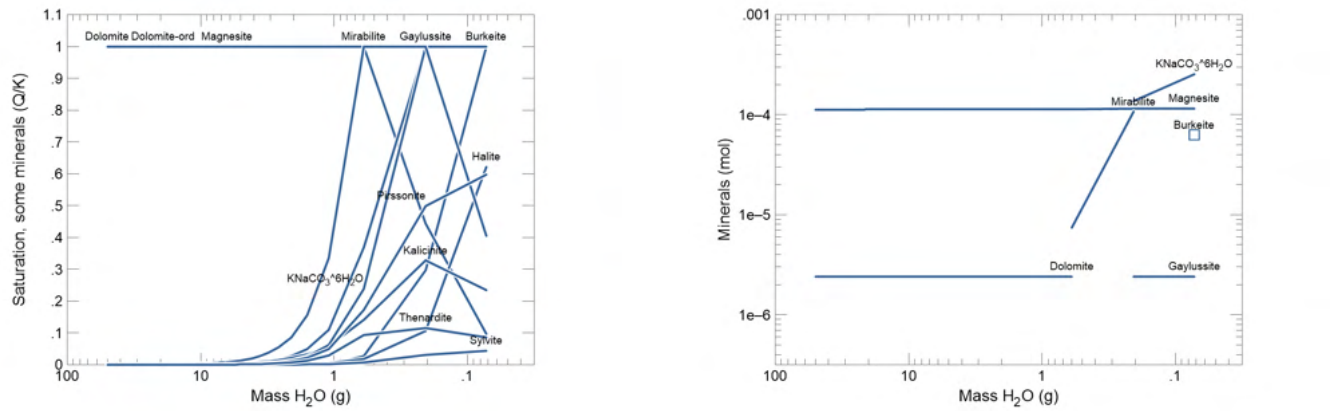

(a) Change in chemical components.

(b) Change in mineral saturation state.

FIGURE 10 Evaporative modeling of Milk Lake surface water. Initial mass of water is 50g, with 1 g being removed every day for 49.9 days. Initial concentrtations are averaged across three samples with the three lowest average [Na^+] and [ALK].

in fact, most metabolic processes seen in soil have similar trends to that of seawater but in much smaller depth intervals. The first mm to cm of sediment is just oxygenated enough to allow for aerobic respiration. Once this oxygen is depleted, microbes must resort to more radical metabolisms (Amenabar, Colman, Poudel, Roden, and Boyd (2018); Sharrar et al. (2020); Wang, sheng Bai, Yang, Zhang, and gang Luo (2023); Xie et al. (2022); Yang, Coppi, Lovley, and Sun (2010)). Aside from impressive resiliency in the absence of no oxygen, these metabolisms produce waste products that may be used in the formation of minerals. At the very least, they give an idea of differences between biological conditions at the surface and within the sediments.

Even away from the surface, evaporation is still a driver in ion concentration, if we continue to use Na^+ as a proxy (Fig.7). However, the difference in Goodenough Lake cores at greater depths suggests a freshwater influx at the site of the orange core.

NH_4^+ follows a depth trend that indicates great biological influence. They correspond to NH_4^+ trends seen in the Saanich Inlet water column, an anoxic fjord basin in British Columbia (Bourbonnais, Lehmann, Hamme, Manning, and Juniper (2013)), with peaks associated at 5-7 cm and 10-12 cm. The first peak can be attributed to a maximum of anaerobic ammonification, where NH_4^+ is released as a waste product and broken down (Emerson and Hamme (2022)). The second lower peak is caused by anaerobic nitrogen fixation, where N_2 is converted to NH_4^+ (Canfield et al. (2010); Lam and Kuypers (2011)). While NH_4^+ and to a greater extent N is not directly involved in mineral formation, it is a macronutrient required by all organisms and serves as fuel for many extremophiles.

Mg^{2+} soil trends are likely influenced by mineral precipitation and biological uptake. In Milk Lake, the rapid decrease from a high initial concentration is likely due to Mg-carbonate and Mg-Na-carbonate formation. Some of it may also be attributed to biological uptake considering Mg serves as a micronutrient for the formation of porphoryn photosynthetic cofactors (Dąbrowski et al. (2010); Rogers, Dari, and Schroeder (2019)), although it is likely impossible for light to penetrate through the top 3 cm of soil. The slight increase with depth may be due to upwelling groundwater, which would bring Mg^{2+} to the lake through water-rock interactions with the underlying Chilcoltin flow basalt (Bevier (1983)). As it travels further up the soil column, the processes mentioned above may remove it from solution. Compared to Milk Lake, Goodenough Lake's steady, decreasing trend of Mg^{2+} may be due to further biological uptake, however, there is no information on the use of Mg as a center for a cellular complex cofactor. Instead, deeper soil conditions may make the formation of Mg-carbonates and Mg-precipitates more kinetically favorable.

Ca^{2+} appear to be the most variable, in error and in depth. The lower range of Ca^{2+} when compared to Mg^{2+} suggest that throughout the entirety of Milk Lake and Goodenough Lake are influenced by the same Ca^{2+} outflux. Ca^{2+} is not as biologically involved as Mg^{2+}, but it is much more susceptible to forming carbonate minerals, and roughly decreases with depth. Between lakes, Milk appears to start out with a higher concentration that decreases while Goodenough stays relatively constant throughout depth. This may be due to Milk Lake being in contact with the neighboring Alberta Lake and other smaller bodies of water(Fig. 1 a), which may supply the surface waters and sediment-water interface with Ca^{2+}. Goodenough Lake has no surrounding body

of water to leach Ca^{2+} from. It also somewhat follows the trend of Mg^{2+}, suggesting that the decrease is also due to Mg-carbonate and Mg-precipitate formation (Daye et al. (2019); Pan et al. (2021)).

4.3 | Alkaline Microbiomes

As we begin to see the importance of both abiotic and biotic processes for the formation of these alkaline lakes, it is important that we find out how alkaline microbes live and how they evolved into their current state. Even without using genomics for phylogenetic identification, light and scanning electron microscopy illuminated how wide the range of microbial morphologies was, and how tightly linked they are to the formation of precipitate minerals; we were even able to identify one genus by eye alone. The Spirogyra genus is thought to be an efficient sink for heavy metals (Gupta and Rastogi (2008)), and in Figure 3 e we can find a radiating mineral formation in association with the cell wall. We can also find much larger crystals growing in association with mats shown in Figure 3 c. It is, however, difficult to ascertain whether these instances of mineral formation are caused by the local algae, or are simply correlated.

4.4 | Precipitation Experiments and The Importance of Ethanol

Through our in-lab experimentation, we were able to show how our system reacted in the presence of different nucleation seeds (Molnár et al. (2021); Pan et al. (2021)) and how our systems equilibrated when Ca^{2+} was introduced through the precipitation of Ca-minerals. Most interestingly, we saw the effects of high percent organic solvents on mineral formation. Over the course of six weeks, we were able to see how the additional of EtOH effectively removed almost all analytes, greatly increased pH, and allowed for the formation of uniquely shaped minerals. In particular, we were able to show that Mg was made more reactive via the adsorption of EtOH and the removal of surrounding water, which has been understood historically as the mechanism in which dolomite precipitation is inhibited (Fang, Zhang, Farfan, and Xu (2022)). While no dolomite was found in our experiments (likely due to lower than necessary Ca^{2+} concentrations), EDS results confirmed the greater formation of Mg-precipitates in EtOH-spiked samples. When compared to the Mg hotspots on non-EtOH samples, the crystals are much larger and much more abundant in Mg. They also often coupled with sodium instead of Ca, suggesting that sodium may be more kinetically favorable in high % EtOH solutions, although this was inconsistent across technical replicates.

5 | CONCLUSIONS

While there appears to be a correlation between alkaliphile mats and mineral precipitation (even with secondary minerals), we have not shown a causative mechanism for the formation of microbially-mediated minerals. However, with our secondary minerals, we have found that certain organic solvents in high concentrations mediate the formation of hard-to-form precipitates and that they may serve as intermediates to or poorly organized variants of hard-to-form carbonates. We suggest further investigations on microbial mat metabolisms and the organic solvents they may produce, the possibility of hard-to-form precipitates in lower concentrations of organic solvents, and more rigorous elemental and structural comparisons between precipitates forming *in situ* with microbial mats and precipitates forming along the dried lakeshore. In addition, we suggest applying genomics (Vavourakis et al. (2016)) and more rigorous microscopy on Caribou Plateau microbial mats so that we may ascertain the relevance of individual physiology (Raudsepp et al. (2024)) and phylogeny (Zorz et al. (2019)) in the grander microbial community.

6 | ACKNOWLEDGEMENTS

As those who live on unceded lands and territories, we acknowledge and respect the Lekwungen (Songhees and Esquimalt) Peoples on whose territory the University of Victoria stands, and the Lekwungen and Saanich Peoples who historical relationships with the land continue to this day.

We also acknowledge and respect Secwepemcúlecw, the land on which we sampled and studied, and the land on which the Secwépemc First Nations continue to live on to this day.

We would like to thank University of Victoria PhD candidates Stacey Edmondsond and Daniel Garduño Ruiz, and Dr. Harold J. Bradbury from the University of British Columbia for assistance in the field. We would also like to thank Dr. Elaine Humphrey

and the Advanced Microscopy Facility for assistance with electron imaging and spectroscopy, as well as Jodie Klymak, Noa Hardcastle, Dr. Andrew Fraas, and Dr. Jay Cullen of the School of Earth and Ocean Science, University of Victoria, for assistance with processing samples in-house. Lastly, a personal thank you Dr. Anne-Sofie Ahm for supervising this project and mentoring me through the process. This work was supported with funding from the University of Victoria's Jamie Cassels Undergraduate Research Award program.

6.1 | Bibliography

References

Amenabar, M. J., Colman, D. R., Poudel, S., Roden, E. E., & Boyd, E. S. (2018, 7). Electron acceptor availability alters carbon and energy metabolism in a thermoacidophile. *Environmental Microbiology*, *20*, 2523-2537. doi: 10.1111/1462-2920.14270

Anderson, R. G., Resnick, J., Russell, J. K., Woodsworth, G. J., Villeneuve, M. E., & Grainger, N. C. (2001, 4). The cheslatta lake suite: Miocene mafic, alkaline magmatism in central british columbia. *Canadian Journal of Earth Sciences*, *38*.

Arvidson, R. S. (1999, 4). The dolomite problem; control of precipitation kinetics by temperature and saturation state. *American Journal of Science*, *299*, 257-288. doi: 10.2475/ajs.299.4.257

Bevier, M. L. (1983, 4). Regional stratigraphy and age of chilcotin group basalts, south-central british columbia. *Canadian Journal of Earth Sciences*, *20*, 515-524. doi: 10.1139/e83-049

Bourbonnais, A., Lehmann, M. F., Hamme, R. C., Manning, C. C., & Juniper, S. K. (2013, 12). Nitrate elimination and regeneration as evidenced by dissolved inorganic nitrogen isotopes in saanich inlet, a seasonally anoxic fjord. *Marine Chemistry*, *157*, 194-207. doi: 10.1016/j.marchem.2013.09.006

Brady, A. L., Druschel, G., Leoni, L., Lim, D. S. S., & Slater, G. F. (2013, 9). Isotopic biosignatures in carbonate-rich, cyanobacteria-dominated microbial mats of the <scp>c</scp> ariboo <scp>p</scp> lateau, <scp>b.c.</scp>. *Geobiology*, *11*, 437-456. doi: 10.1111/gbi.12050

Canfield, D. E., Stewart, F. J., Thamdrup, B., Brabandere, L. D., Dalsgaard, T., Delong, E. F., … Ulloa, O. (2010). A cryptic sulfur cycle in oxygen-minimum-zone waters off the chilean coast. *Science*, *330*. doi: 10.1126/science.1196889

Daye, M., Higgins, J., & Bosak, T. (2019, 6). Formation of ordered dolomite in anaerobic photosynthetic biofilms. *Geology*, *47*, 509-512. doi: 10.1130/G45821.1

Deutsch, W. J., Jenne, E. A., & Krupka, K. M. (1982, 6). Solubility equilibria in basalt aquifers: The columbia plateau, eastern washington, u.s.a. *Chemical Geology*, *36*, 15-34. doi: 10.1016/0009-2541(82)90037-7

Dickson, A., Chris, S., & Christian, J. R. (2007, 4). Guide to best practices for ocean co2 measurements. *Guide to Best Practices for Ocean CO2 Measurements*, *3*.

Dąbrowski, J. M., Arnaut, L. G., Pereira, M. M., Monteiro, C. J. P., Urbańska, K., Simões, S., & Stochel, G. (2010, 10). New halogenated water-soluble chlorin and bacteriochlorin as photostable pdt sensitizers: Synthesis, spectroscopy, photophysics, and in vitro photosensitizing efficacy. *ChemMedChem*, *5*, 1770-1780. doi: 10.1002/cmdc.201000223

Eljalafi, A., & Sarg, J. F. (2021, 6). Depositional system and lake-stage control on microbialite morphology, green river formation, eastern uinta basin, colorado and utah, u.s.a. *Journal of Sedimentary Research*, *91*, 636-661. doi: 10.2110/jsr.2020.073

Emerson, S. R., & Hamme, R. C. (2022). *Chemical oceanography*. Cambridge University Press. doi: 10.1017/9781316841174

Engel, A. (1978, 1). Molecular weight determination by scanning transmission electron microscopy. *Ultramicroscopy*, *3*, 273-281. doi: 10.1016/S0304-3991(78)80037-0

Fang, Y., Zhang, F., Farfan, G. A., & Xu, H. (2022, 1). Low-temperature synthesis of disordered dolomite and high-magnesium calcite in ethanol–water solutions: The solvation effect and implications. *ACS Omega*, *7*, 281-292. doi: 10.1021/acsomega.1c04624

Gupta, V., & Rastogi, A. (2008, 3). Biosorption of lead from aqueous solutions by green algae spirogyra species: Kinetics and equilibrium studies. *Journal of Hazardous Materials*, *152*, 407-414. doi: 10.1016/j.jhazmat.2007.07.028

Haines, M., Khot, V., & Strous, M. (2023, 2). The vigor, futility, and application of microbial element cycles in alkaline soda lakes. *Elements*, *19*, 30-36. doi: 10.2138/gselements.19.1.30

Heim, C. (2011). Microbial biomineralization. In (p. 586-592). doi: 10.1007/978-1-4020-9212-1_33

Keul, N., Morse, J. W., Wanninkhof, R., Gledhill, D. K., & Bianchi, T. S. (2010, 6). Carbonate chemistry dynamics of surface

waters in the northern gulf of mexico. *Aquatic Geochemistry*, *16*, 337-351. doi: 10.1007/s10498-010-9091-2

Klein, C., & Philpotts, A. (2016). *Earth materials 2nd edition*. Cambridge University Press. doi: 10.1017/9781316652909

Lam, P., & Kuypers, M. M. (2011). Microbial nitrogen cycling processes in oxygen minimum zones. *Annual Review of Marine Science*, *3*. doi: 10.1146/annurev-marine-120709-142814

Land, L. S. (1998). Failure to precipitate dolomite at 25 c from dilute solution despite 1000-fold oversaturation after 32 years. *Aquatic Geochemistry*, *4*, 361-368. doi: 10.1023/A:1009688315854

Li, X., Wang, J., Long, G., Xu, L., Cui, J., Sun, X., & Wang, Y. (2024, 2). Eocene lacustrine microbialites in the western qaidam basin, china: implication for the sedimentary record and hydrocarbon potential. *Carbonates and Evaporites*, *39*, 5. doi: 10.1007/s13146-023-00911-8

Molnár, Z., Pekker, P., Dódony, I., & Pósfai, M. (2021, 8). Clay minerals affect calcium (magnesium) carbonate precipitation and aging. *Earth and Planetary Science Letters*, *567*, 116971. doi: 10.1016/j.epsl.2021.116971

Nichols, F., Pontefract, A., Dion-Kirschner, H., Masterson, A. L., & Osburn, M. R. (2023, 10). Lipid biosignatures from so ₄ -rich hypersaline lakes of the cariboo plateau. *Journal of Geophysical Research: Biogeosciences*, *128*. doi: 10.1029/2023JG007480

Noffke, N., Eriksson, K. A., Hazen, R. M., & Simpson, E. L. (2006). A new window into early archean life: Microbial mats in earth's oldest siliciclastic tidal deposits (3.2 ga moodies group, south africa). *Geology*, *34*, 253. doi: 10.1130/G22246.1

Pan, Y., Li, Y., Ma, Q., He, H., Wang, S., Sun, Z., … Chen, C.-T. A. (2021, 12). The role of mg2+ in inhibiting caco3 precipitation from seawater. *Marine Chemistry*, *237*, 104036. doi: 10.1016/j.marchem.2021.104036

Peel, M. C., Finlayson, B. L., & Mcmahon, T. A. (2007, 10). Updated world map of the köppen-geiger climate classification. *Hydrol. Earth Syst. Sci*, *11*, 1633-1644. Retrieved from `www.hydrol-earth-syst-sci.net/11/1633/2007/`

Prieto-Barajas, C. M., Valencia-Cantero, E., & Santoyo, G. (2018, 1). Microbial mat ecosystems: Structure types, functional diversity, and biotechnological application. *Electronic Journal of Biotechnology*, *31*, 48-56. doi: 10.1016/j.ejbt.2017.11.001

Raudsepp, M. J., Wilson, S., Zeyen, N., Arizaleta, M. L., & Power, I. M. (2024, 3). Magnesite everywhere: Formation of carbonates in the alkaline lakes and playas of the cariboo plateau, british columbia, canada. *Chemical Geology*, *648*, 121951. Retrieved from `https://linkinghub.elsevier.com/retrieve/pii/S0009254124000317` doi: 10.1016/j.chemgeo.2024.121951

Renaut, R., & Long, P. (1989, 10). Sedimentology of the saline lakes of the cariboo plateau, interior british columbia, canada. *Sedimentary Geology*, *64*, 239-264.

Riding, R. (2011). Microbialites, stromatolites, and thrombolites. In (p. 635-654). doi: 10.1007/978-1-4020-9212-1_196

Rogers, C. W., Dari, B., & Schroeder, K. L. (2019, 1). Comparison of soil-test extractants for potassium, calcium, magnesium, sulfur, and micronutrients in idaho soils. *Agrosystems, Geosciences & Environment*, *2*, 1-9. doi: 10.2134/age2019.08.0067

Sanz-Montero, M. E., & Rodríguez-Aranda, J. P. (2022, 9). Seismites in miocene gypsum microbialites: Multi-proxy tools for paleoenvironmental reconstruction of saline lakes. *Sedimentary Geology*, *439*, 106219. doi: 10.1016/j.sedgeo.2022.106219

Schulze-Makuch, D., Lim, D., Laval, B., Turse, C., António, M., Chan, O., … Irwin, L. (2012, 12). Pavilion lake microbialites: Morphological, molecular and biochemical evidence for a cold-water transition to colonial aggregates. *Life*, *3*, 21-37. doi: 10.3390/life3010021

Sharrar, A. M., Crits-Christoph, A., Méheust, R., Diamond, S., Starr, E. P., & Banfield, J. F. (2020, 6). Bacterial secondary metabolite biosynthetic potential in soil varies with phylum, depth, and vegetation type. *mBio*, *11*. doi: 10.1128/mBio.00416-20

Stoica, C., Verwer, P., Meekes, H., van Hoof, P. J. C. M., Kaspersen, F. M., & Vlieg, E. (2004, 7). Understanding the effect of a solvent on the crystal habit. *Crystal Growth & Design*, *4*, 765-768. doi: 10.1021/cg0342314

Tebbs, E., Remedios, J., Avery, S., Rowland, C., & Harper, D. (2015, 8). Regional assessment of lake ecological states using landsat: A classification scheme for alkaline–saline, flamingo lakes in the east african rift valley. *International Journal of Applied Earth Observation and Geoinformation*, *40*, 100-108. doi: 10.1016/j.jag.2015.03.010

Toggweiler, J. R., & Sarmiento, J. L. (2013, 3). Glacial to interglacial changes in atmospheric carbon dioxide: The critical role of ocean surface water in high latitudes. In (p. 163-184). doi: 10.1029/GM032p0163

Tutolo, B. M., & Tosca, N. J. (2018, 3). Experimental examination of the mg-silicate-carbonate system at ambient temperature: Implications for alkaline chemical sedimentation and lacustrine carbonate formation. *Geochimica et Cosmochimica Acta*,

225, 80-101. doi: 10.1016/j.gca.2018.01.019

Tutolo, B. M., & Tosca, N. J. (2023, 2). Dry, salty, and habitable: The science of alkaline lakes. *Elements*, *19*, 10-14. doi: 10.2138/gselements.19.1.10

Vavourakis, C. D., Ghai, R., Rodriguez-Valera, F., Sorokin, D. Y., Tringe, S. G., Hugenholtz, P., & Muyzer, G. (2016, 2). Metagenomic insights into the uncultured diversity and physiology of microbes in four hypersaline soda lake brines. *Frontiers in Microbiology*, *7*. doi: 10.3389/fmicb.2016.00211

Wang, Y., sheng Bai, D., Yang, X., Zhang, Y., & gang Luo, X. (2023, 5). Soil sulfur cycle bacteria and metabolites affected by soil depth and afforestation conditions in high-sulfur coal mining areas. *Applied Soil Ecology*, *185*, 104802. doi: 10.1016/j.apsoil.2022.104802

White, R. A. (2020, 7). The global distribution of modern microbialites: Not so uncommon after all. In (chap. 5). Springer, Cham. doi: 10.1007/978-3-030-46087-7_5

Xie, Z., Yu, Z., Li, Y., Wang, G., Liu, X., Tang, C., … Jin, J. (2022, 4). Soil microbial metabolism on carbon and nitrogen transformation links the crop-residue contribution to soil organic carbon. *npj Biofilms and Microbiomes*, *8*, 14. doi: 10.1038/s41522-022-00277-0

Yang, T. H., Coppi, M. V., Lovley, D. R., & Sun, J. (2010). Metabolic response of geobacter sulfurreducens towards electron donor/acceptor variation. *Microbial Cell Factories*, *9*, 90. doi: 10.1186/1475-2859-9-90

Yoou, M.-C., Kim, M.-K., & Kim, G.-H. (2009, 3). Conjugation process in spirogyra varians monitored with fitc-lectins(zygnemataceae, chlorophyta). *ALGAE*, *24*, 39-45. doi: 10.4490/ALGAE.2009.24.1.039

Zeebe, R. E., & Wolf-Gladrow, D. (2001). Co2 in seawater: equilibrium, kinetics, isotopes. chapter 1 equilibrium. *Elsevier Oceanography Series*, *65*.

Zorz, J. K., Sharp, C., Kleiner, M., Gordon, P. M. K., Pon, R. T., Dong, X., & Strous, M. (2019, 9). A shared core microbiome in soda lakes separated by large distances. *Nature Communications*, *10*, 4230. doi: 10.1038/s41467-019-12195-5

The normal commands for producing the reference list are:

How to cite this article: Thompson M.O. (2024), Fluid and mineral carbonate biogeochemistry and microbial mats of Caribou Plateau alkaline lakes, *[Unpublished bachelor's thesis]*, University of Victoria.

APPENDIX

A MICROBIAL MAT STRUCTURES

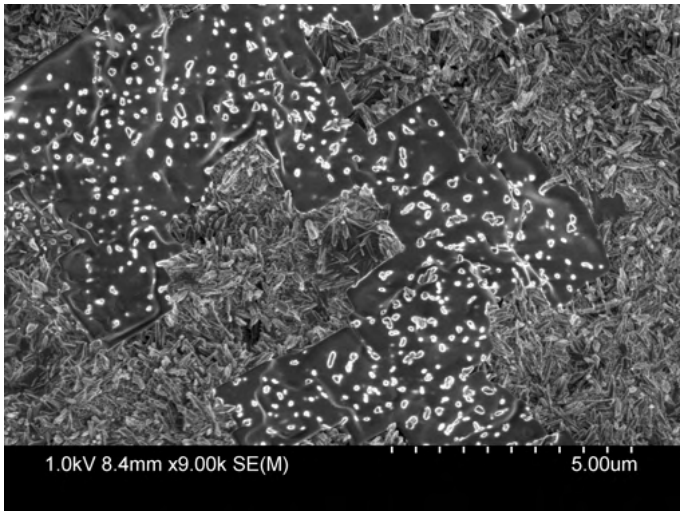

FIGURE A1 Flat object with geometrical perimeter. White spots are holes where nm-scale crystals pierce through

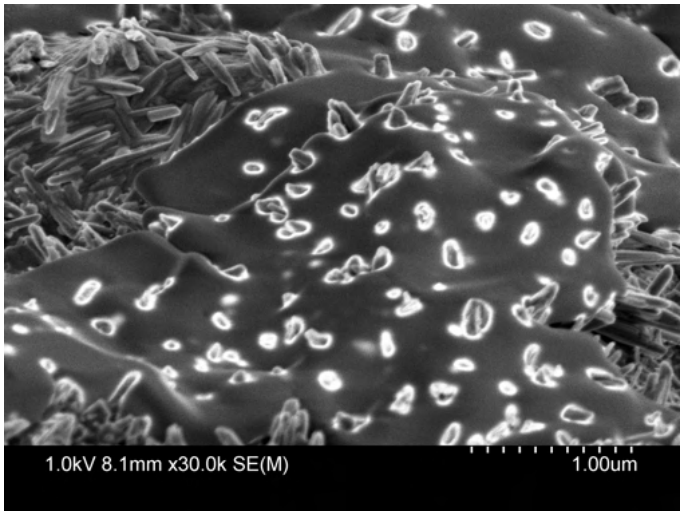

FIGURE A2 Closeup of unknown geometrical object being pierced by nm-scale crystals

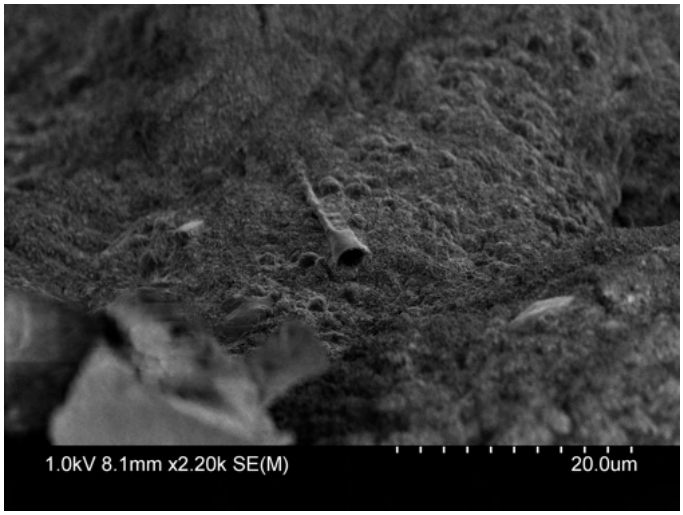

FIGURE A3 Empty biological casing

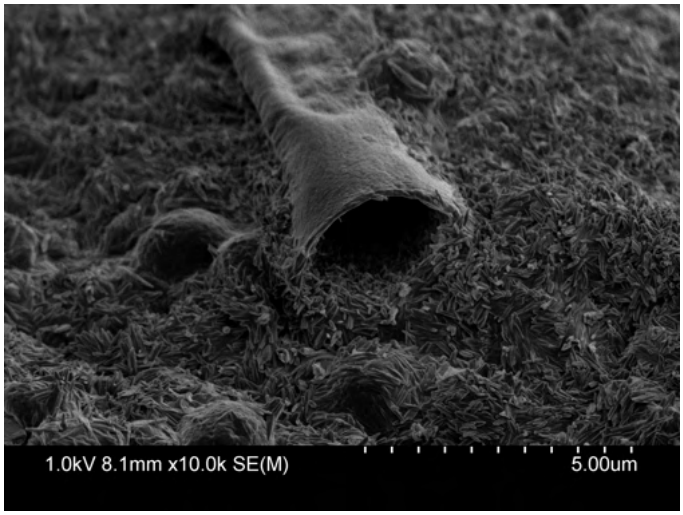

FIGURE A4 Empty biological casing with nm-scale crystals and μm-sacle mineral nodules

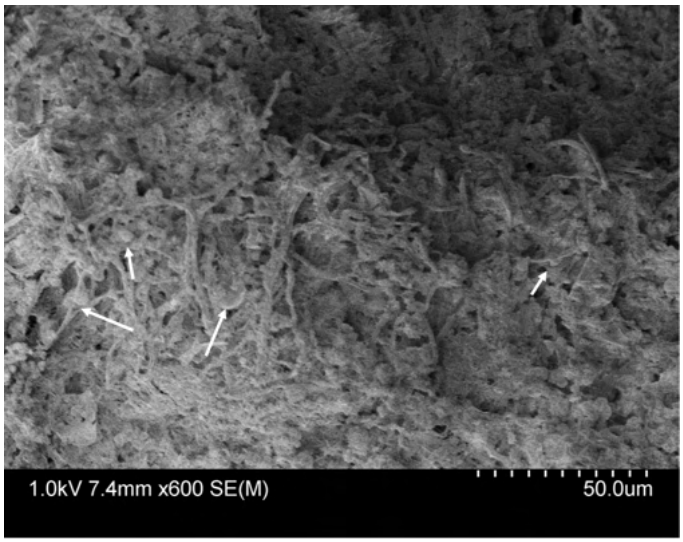

FIGURE A5 Fibrous algae tangled with each other. Arrows point to rounded growths found sporadically throughout micrograph

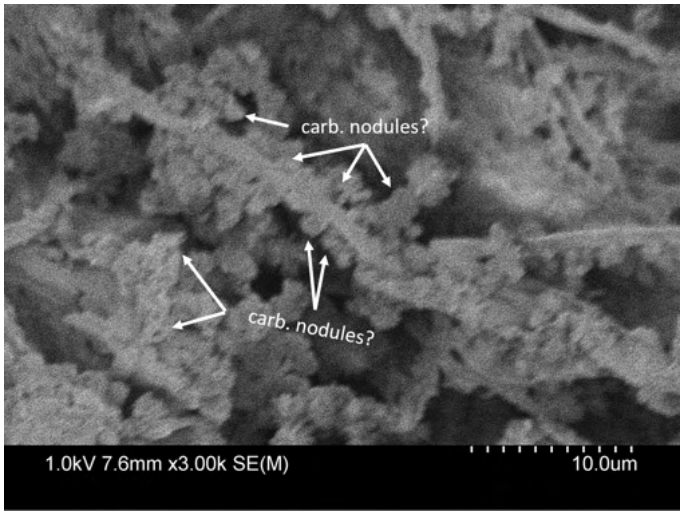

FIGURE A6 Fibrous algae with crystalline growths along cell length

B ENCRUSTED SOIL SAMPLES

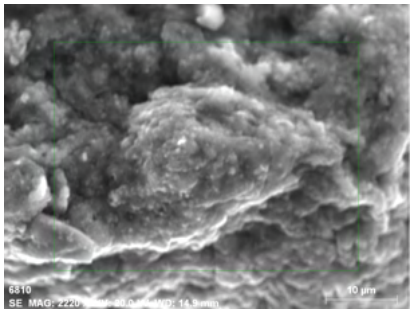

(a) Micrograph

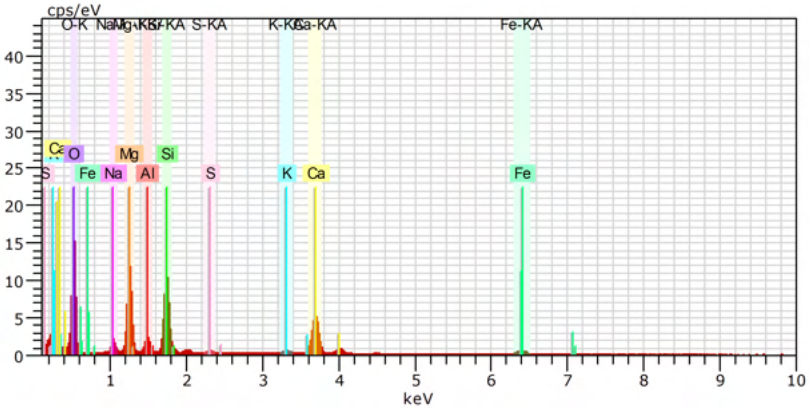

(b) EDS spectrum

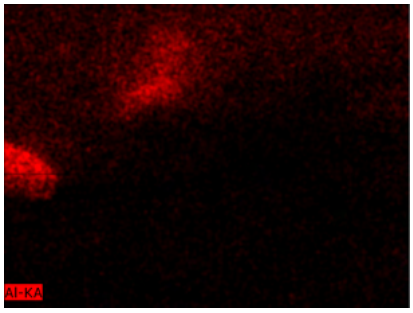

(c) Al map

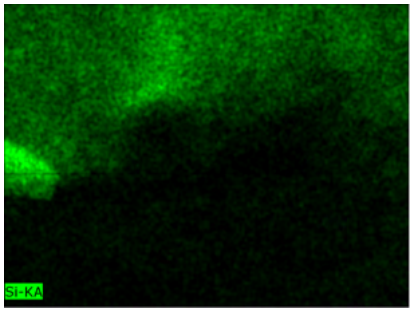

(d) Si map

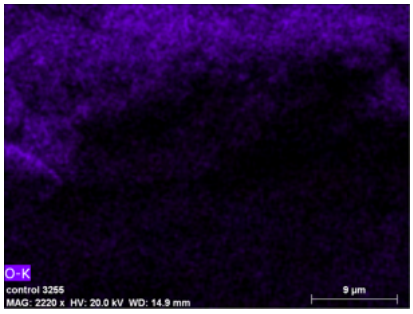

(e) O map

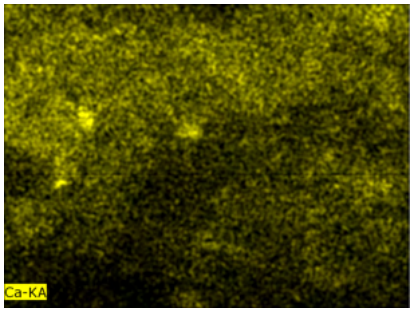

(f) Ca map

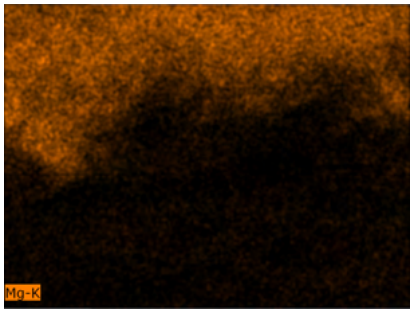

(g) Mg map

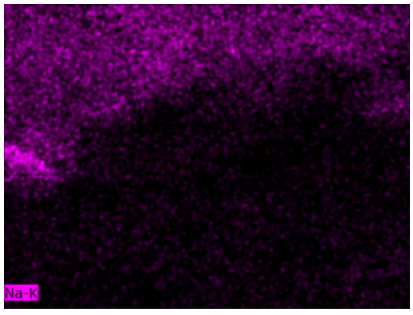

(h) Na map

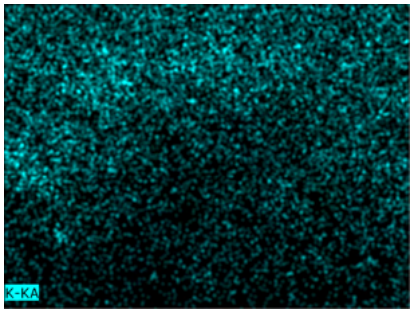

(i) K map

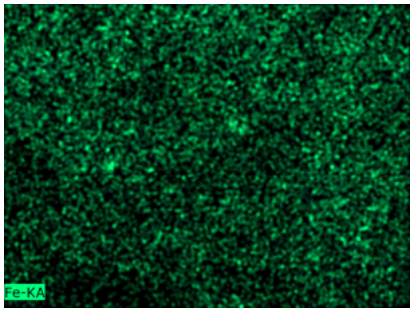

(j) Fe map

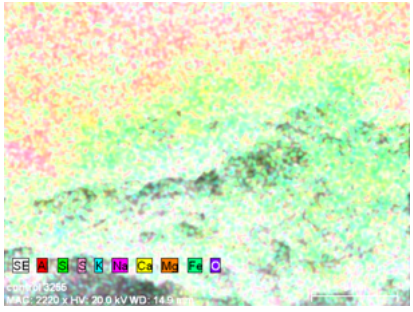

(k) Elemental map

FIGURE B7 EDS Elemental map of Goodenough Lake precipitate experiment sample. Seed: Kaolinite. Solution: 90% EtOH

C SURFACE WATER SAMPLES

	Normalized Alkalinity (meq/mmol)	Normalized DIC	Field pH	Initial pH	Salinity (ppt)
MILK1	1.04	0.71	9.9	10.1	6.14
MILK2	1.02	0.643	9.9	9.97	5.53
MILK3	1.05	0.701	9.9	9.84	5.35
MILK4	1.06	0.757	9.8	10	5.45
MILK5	1.06	0.797	9.8	9.81	4.81
MILK7	1.04	0.73	9.9	10	5.06
MILK8	1.08	0.762	9.7	9.82	5.18
MILK9	1.05	0.751	9.8	9.97	4.93
MILK10	1.01	0.133	9.9	9.92	6.17
MILK11	1.02	0.678	9.8	9.95	5.09
MILK12	1.04	0.773	10.1	10	4.97
MILK13	0.979	0.000318	10.1		10.3
MILK14	1.02	0.714	9.9	10	10.6
MILK15	10.7	0.617	9.9	9.89	5.36
MILK16	1	0.705	10.0	10.2	7.86
MILK17	1.01	0.703	10.0	10	5.69
MILK18	1.02	0.707	10.0	10.2	6.98
MILK19	1.01	0.53	9.8	10	7.44
MILK20	1.02	0.691	9.9		5.37
GEL1	0.902	0.483	10.3	10.3	22.2
GEL2	1.24	1.42	9.4	9.24	2.16
GEL3	0.892	0.673	10.2	10.3	22.6
GEL4	0.912	0.51	10.1	10.4	21.4

TABLE C1 Surface water chemical properties. MILK1-20: Milk Lake surface water, western shore; GEL1-4: Goodenough Lake surface water, western shore.

	Na^+ (mmol/L)	NH_4^+ (umol/L)	Mg^{2+} (mmol/L)	Ca^{2+} (umol/L)	SO_4^{2-} (mmol/L)
MILK1	132	2.22	15.8	1.04	0.0183
MILK2	121	0.506	19.2	0.388	0.0216
MILK3	116	0.227	21.7	0.375	0.0224
MILK4	122	0.238	21.5	0.352	0.023
MILK5	102	0.196	25.1	0.407	0.0233
MILK7	116	0.242	22.4	0.356	0.0231
MILK8	111	-	21.1	0.354	0.0239
MILK9	112	0.243	23.1	0.361	0.023
MILK10	130	-	20.2	0.373	0.022
MILK11	116	0.266	16.9	0.548	0.0201
MILK12	115	0.294	16.8	0.566	0.0206
MILK13	242	0.145	9.45	0.189	0.0275
MILK14	252	0.223	11.3	0.237	0.0219
MILK15	120	-	19.5	0.349	0.0239
MILK16	173	0.316	14	0.267	0.0214
MILK17	127	0.202	17.9	0.361	0.0205
MILK18	158	-	15.4	0.324	0.021
MILK19	171	-	14.6	0.275	0.0212
MILK20	121	-	16.5	0.568	0.0203
GEL1	536	0.498	3.75	0.168	0.158
GEL2	41.4	10.5	120	1.24	-
GEL3	552	1.16	3.55	0.135	0.162
GEL4	538	0.196	3.7	0.155	0.156

TABLE C2 Na^+ and Na^+ normalized ion concentrations. MILK1-20: Milk Lake surface water, western shore; GEL1-4: Goodenough Lake surface water, western shore.

D PRECIPITATION EXPERIMENTS

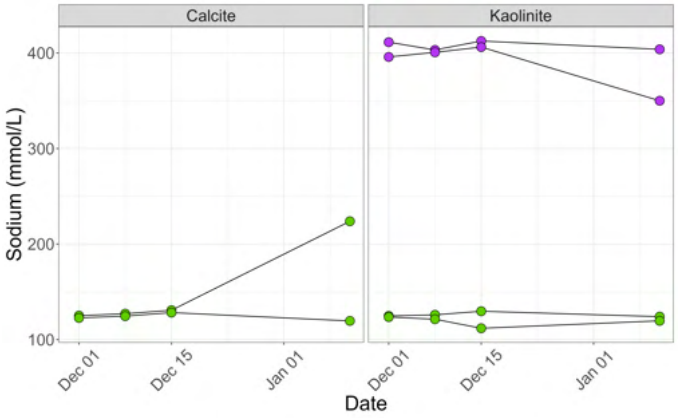

(a) Control Na

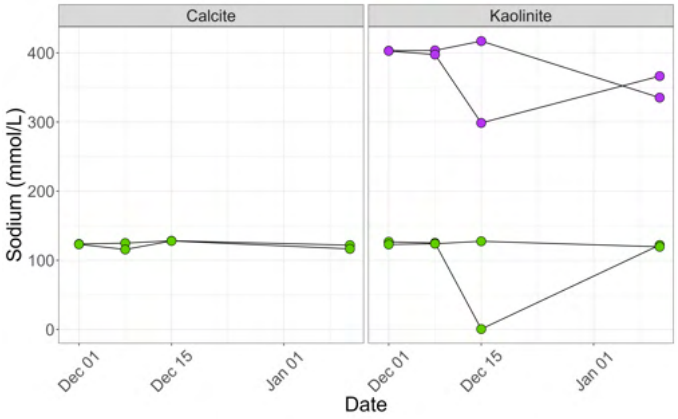

(b) Calcium Na

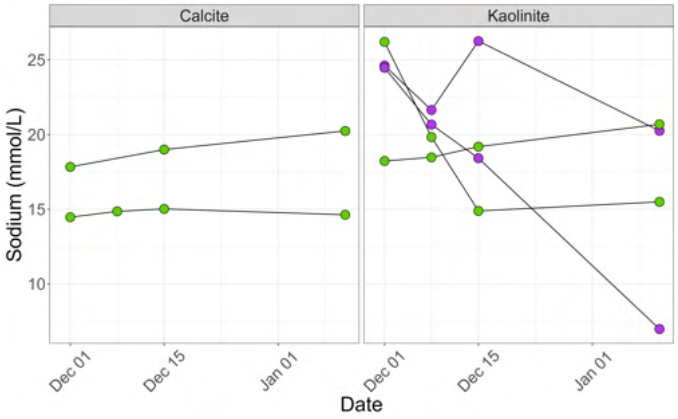

(c) EtOH Na

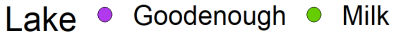

FIGURE D8 pH time series separated by seed.

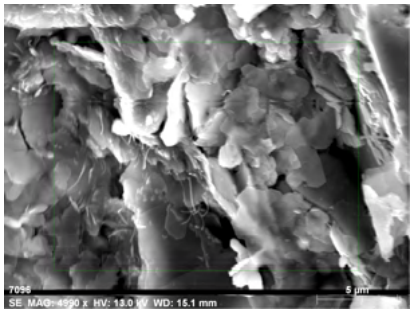

(a) Micrograph

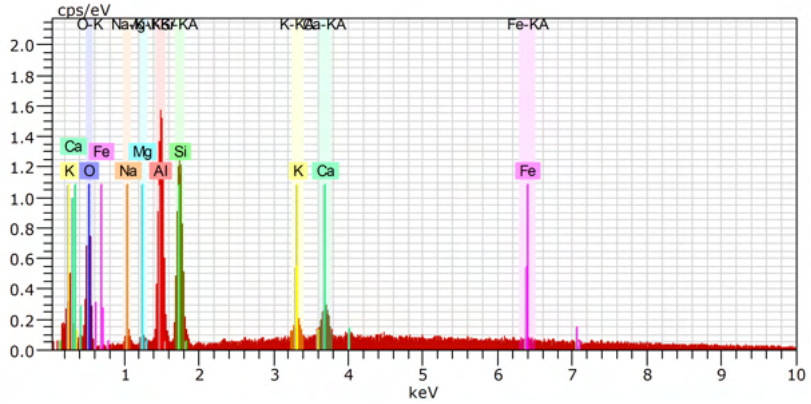

(b) EDS spectrum

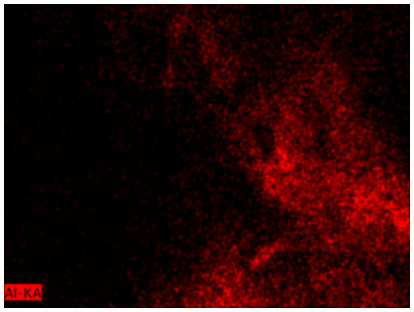

(c) Al map

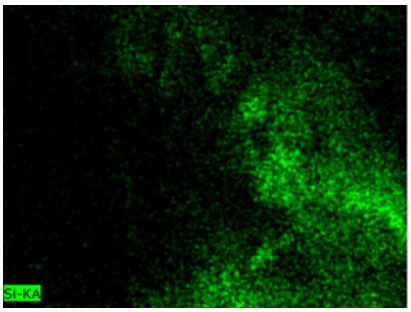

(d) Si map

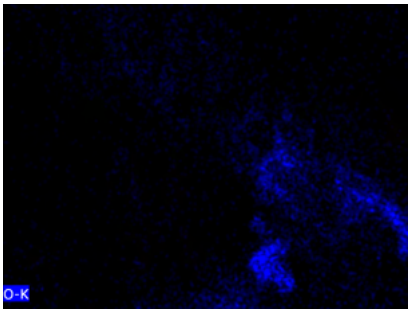

(e) O map

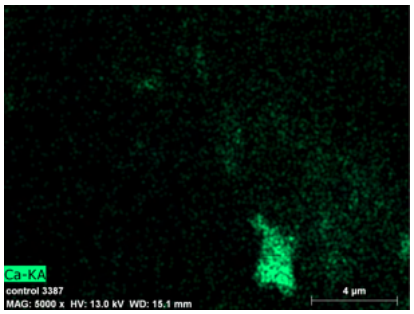

(f) Ca map

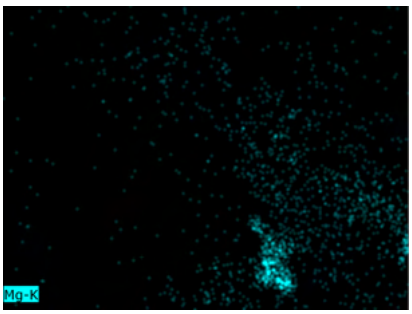

(g) Mg map

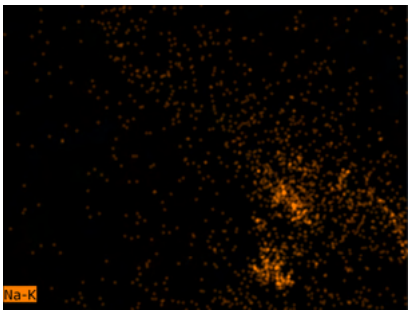

(h) Na map

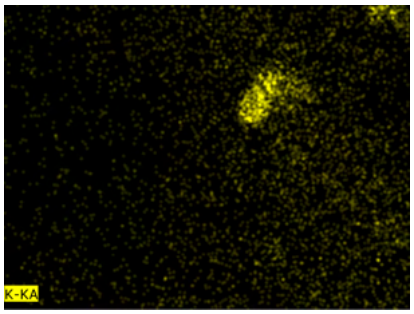

(i) K map

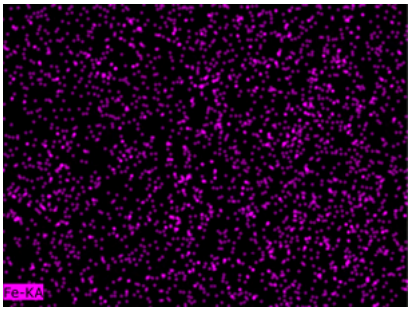

(j) Fe map

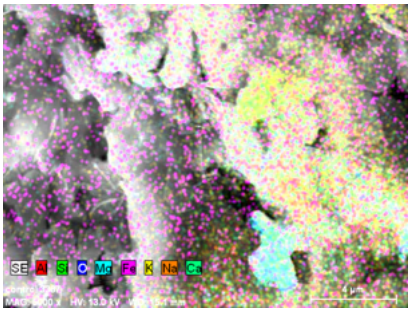

(k) Elemental map

FIGURE D9 EDS Elemental map of Goodenough Lake precipitate experiment sample. Seed: Kaolinite. Solution: 10000ppm Ca

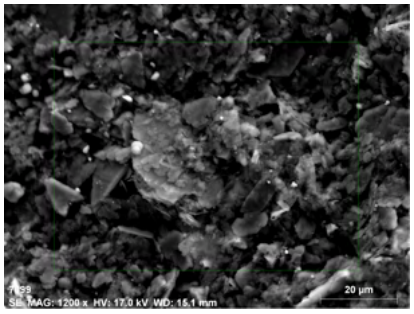

(a) Micrograph

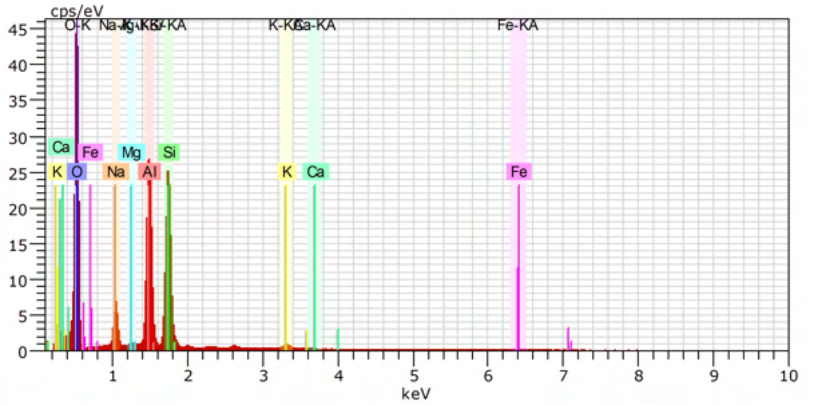

(b) EDS spectrum

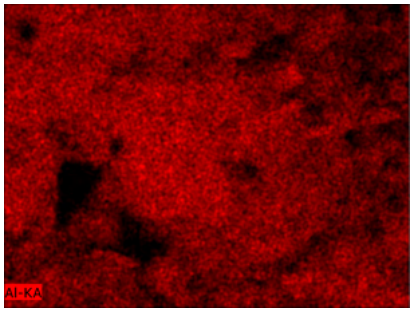

(c) Al map

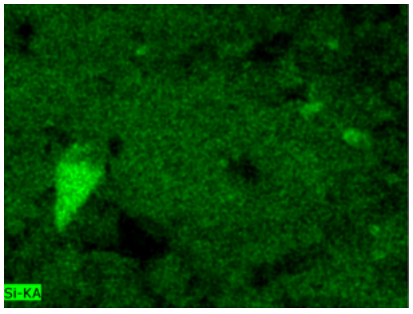

(d) Si map

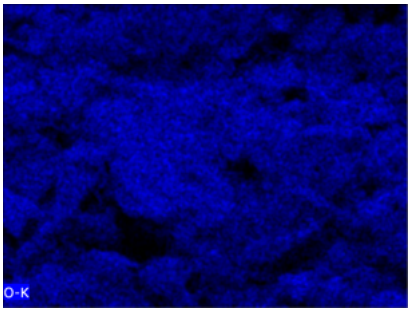

(e) O map

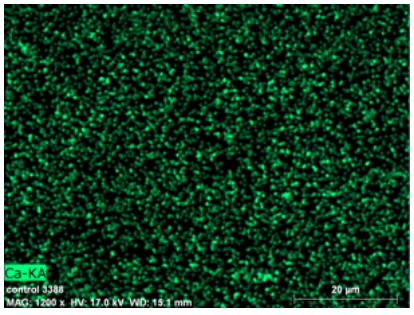

(f) Ca map

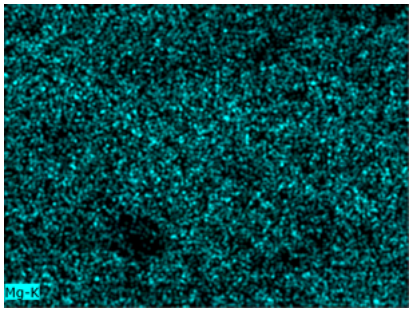

(g) Mg map

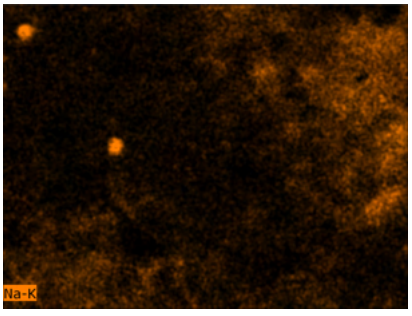

(h) Na map

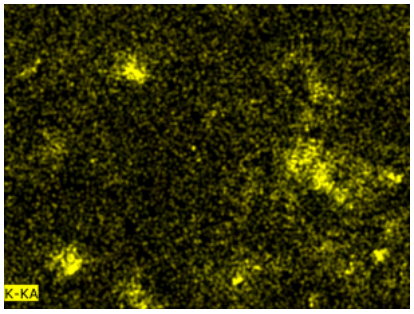

(i) K map

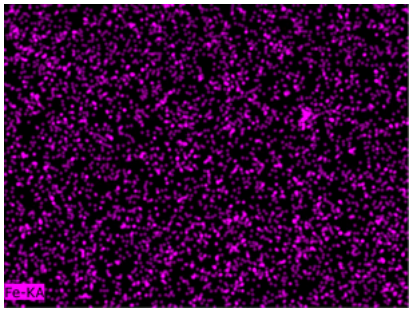

(j) Fe map

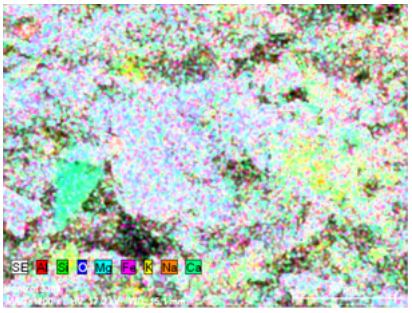

(k) Elemental map

FIGURE D10 EDS Elemental map of Goodenough Lake precipitate experiment sample. Seed: Kaolinite. Solution: None

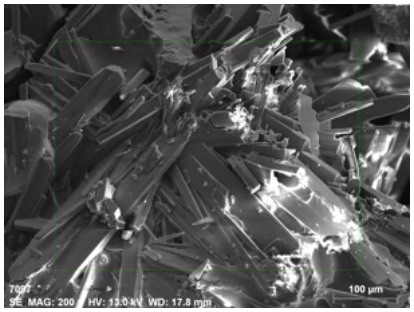

(a) Micrograph

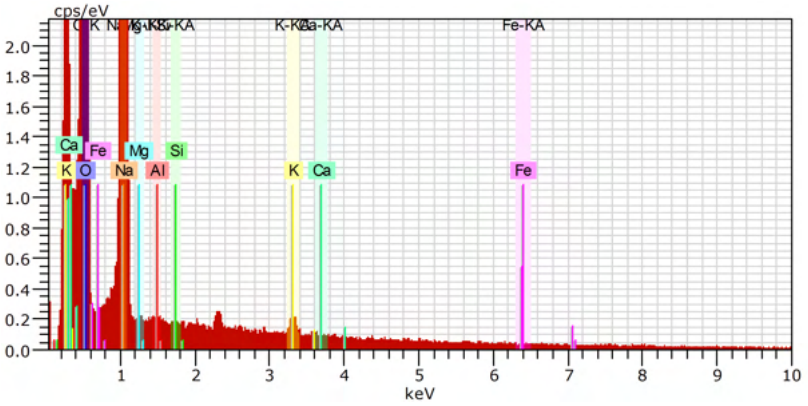

(b) EDS spectrum

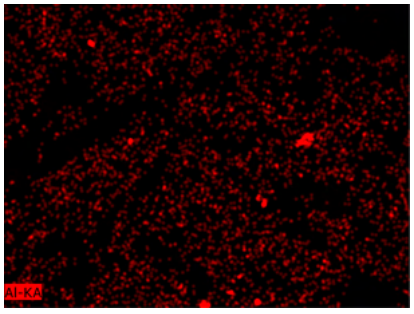

(c) Al map

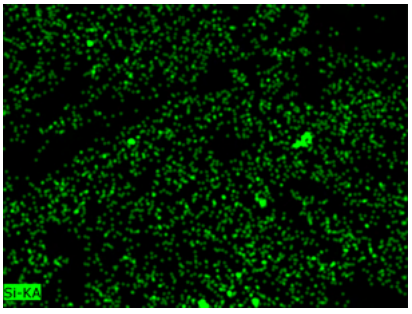

(d) Si map

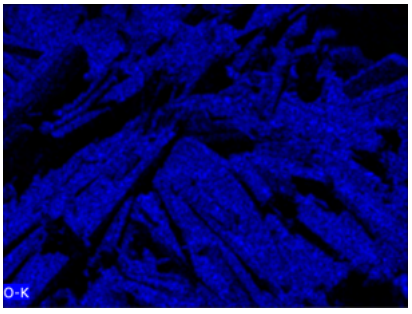

(e) O map

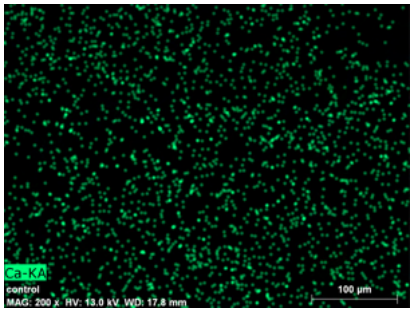

(f) Ca map

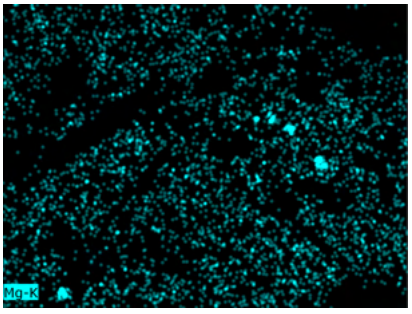

(g) Mg map

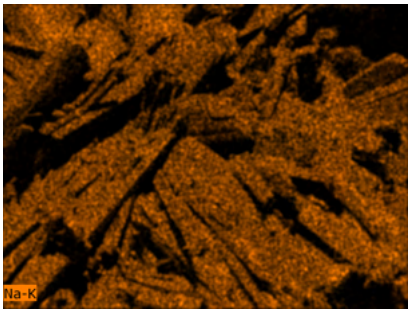

(h) Na map

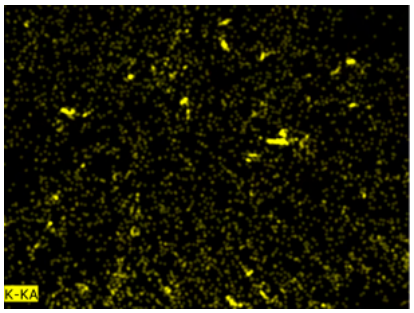

(i) K map

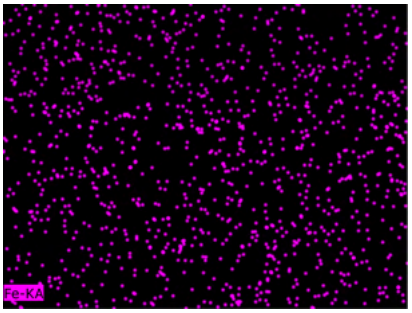

(j) Fe map

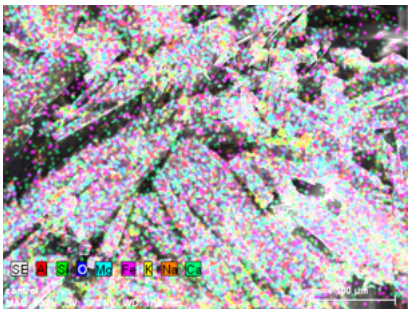

(k) Elemental map

FIGURE D11 EDS Elemental map of Goodenough Lake precipitate experiment sample. Seed: Kaolinite. Solution: 90% EtOH

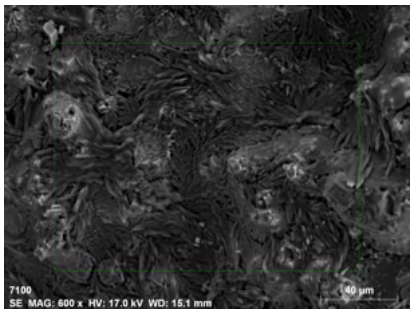

(a) Micrograph

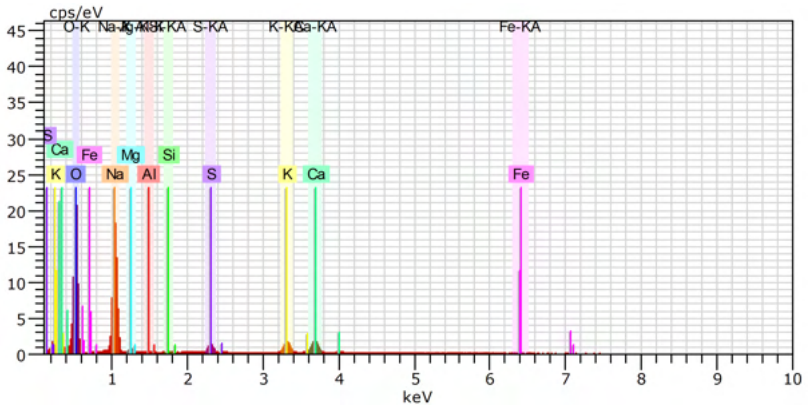

(b) EDS spectrum

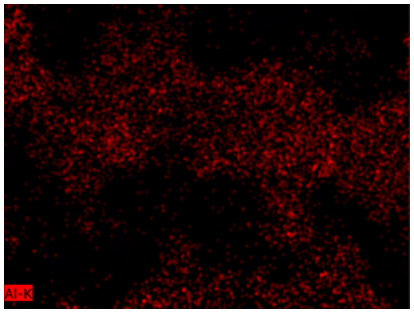

(c) Al map

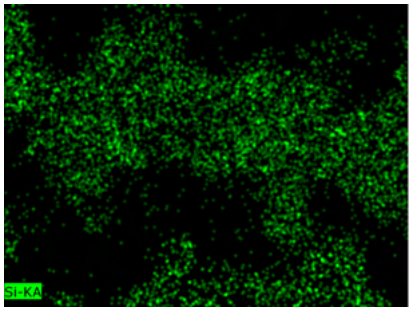

(d) Si map

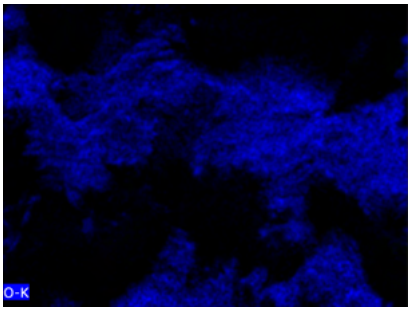

(e) O map

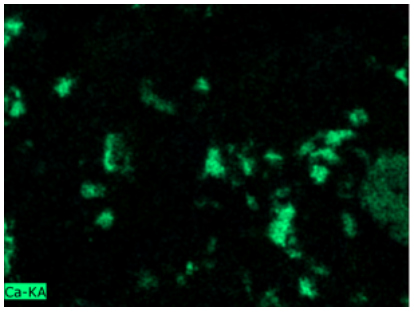

(f) Ca map

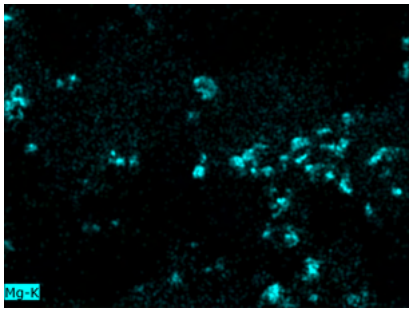

(g) Mg map

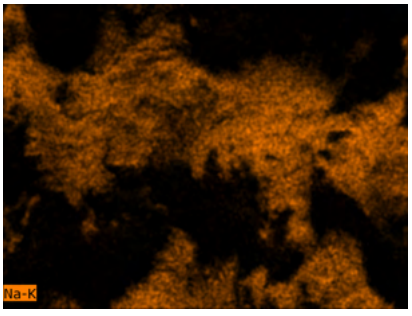

(h) Na map

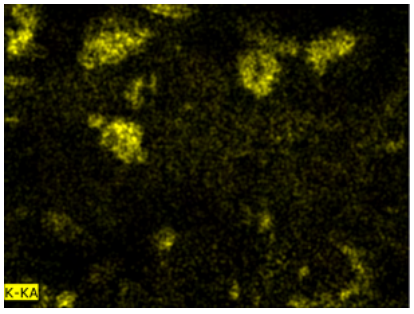

(i) K map

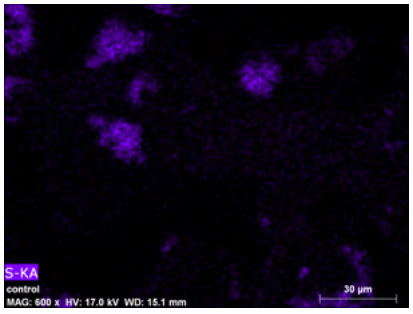

(j) S map

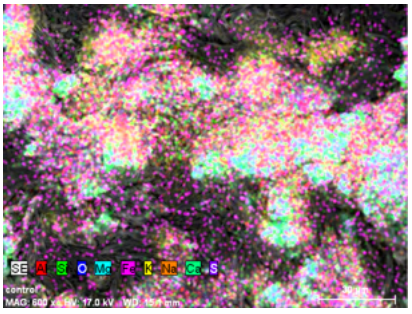

(k) Elemental map

FIGURE D12 EDS Elemental map of Milk Lake precipitate experiment sample. Seed: Calcite. Solution: 90% EtOH

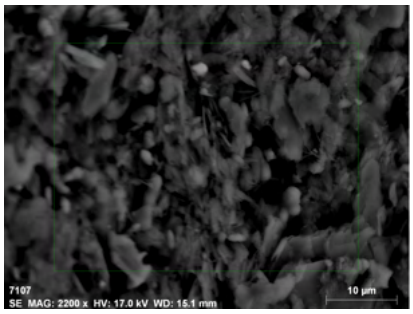

(a) Micrograph

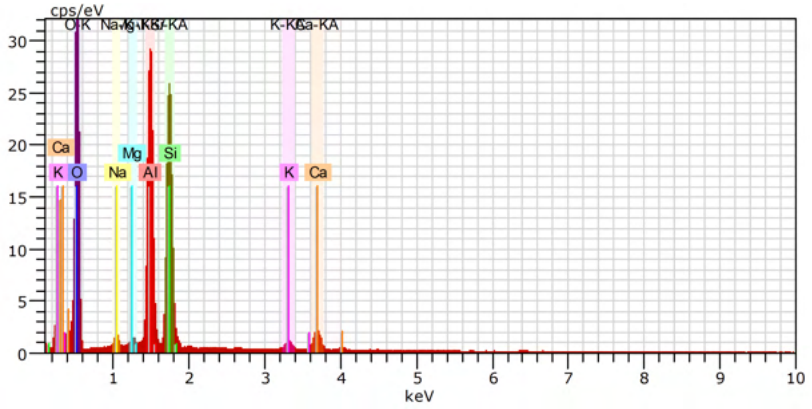

(b) EDS spectrum

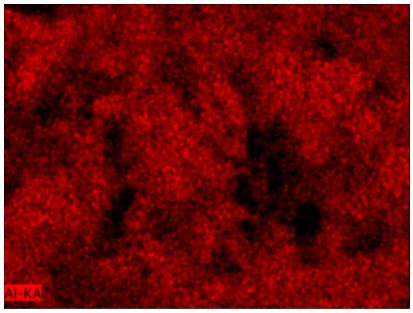

(c) Al map

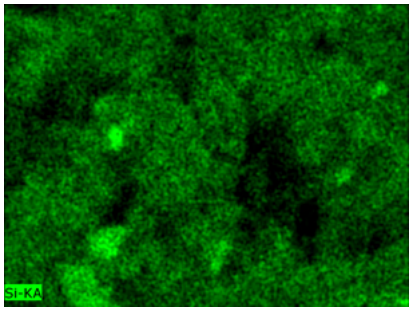

(d) Si map

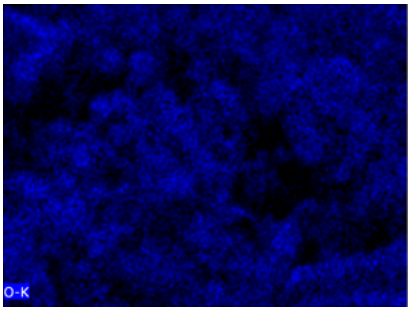

(e) O map

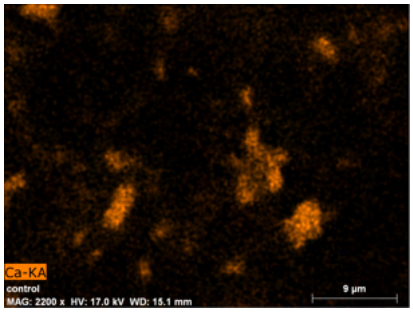

(f) Ca map

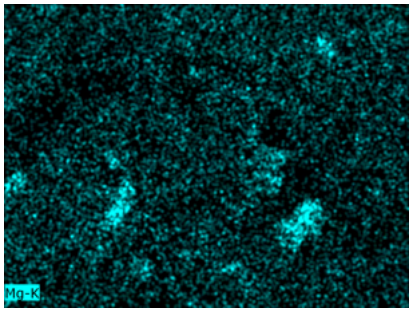

(g) Mg map

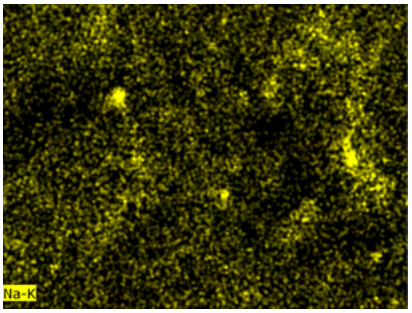

(h) Na map

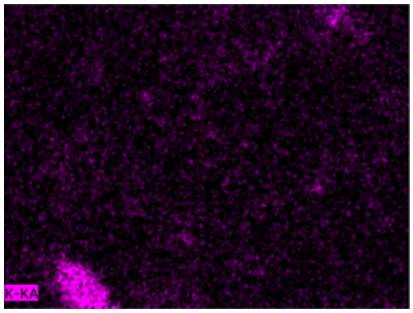

(i) K map

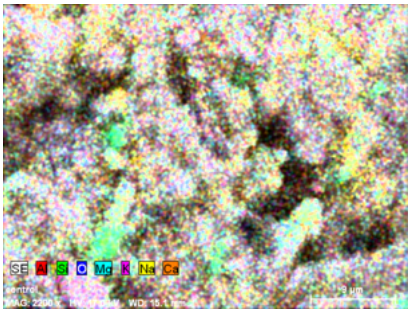

(j) Elemental map

FIGURE D13 EDS Elemental map of Milk Lake precipitate experiment sample. Seed: Kaolinite. Solution: 10000 ppm Ca

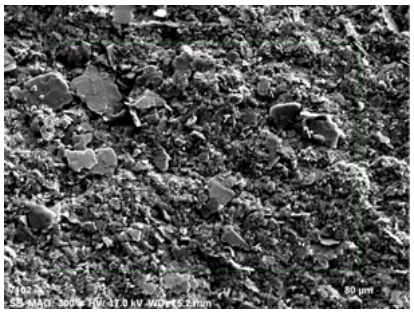

(a) Micrograph

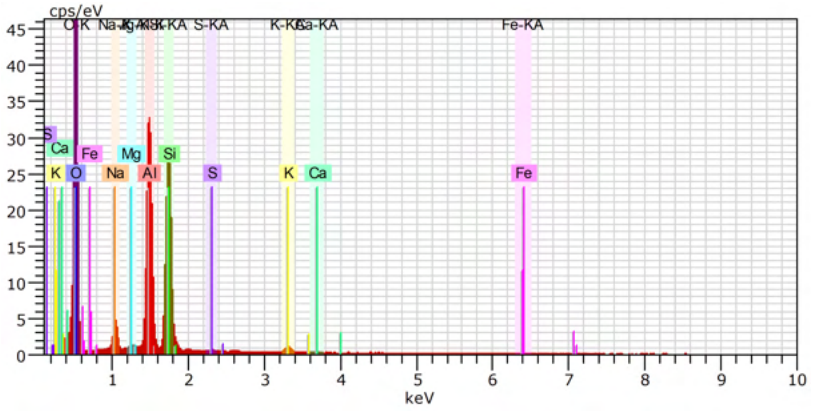

(b) EDS spectrum

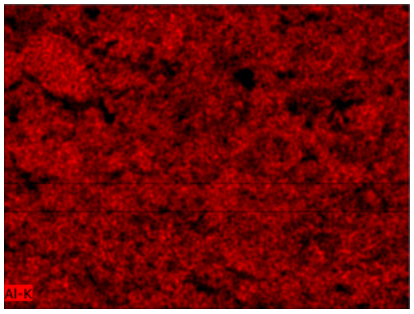

(c) Al map

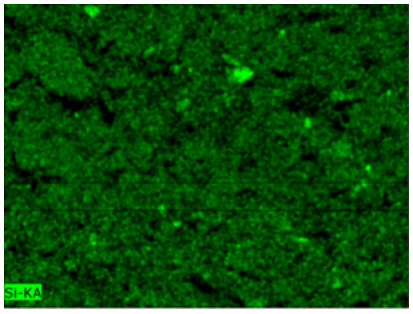

(d) Si map

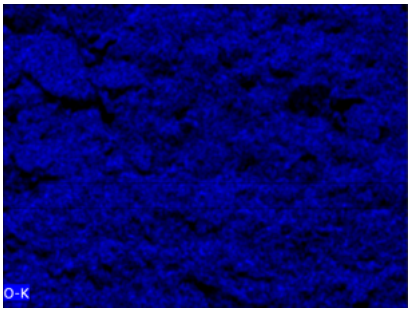

(e) O map

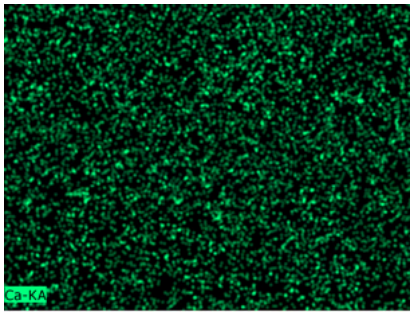

(f) Ca map

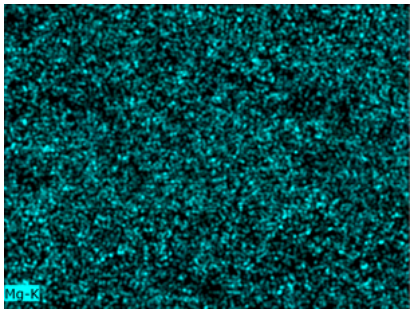

(g) Mg map

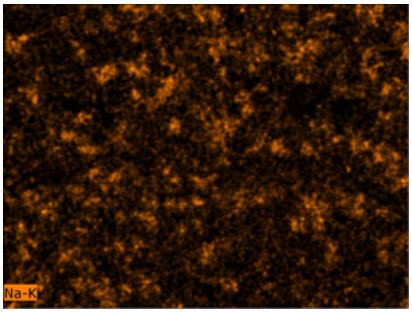

(h) Na map

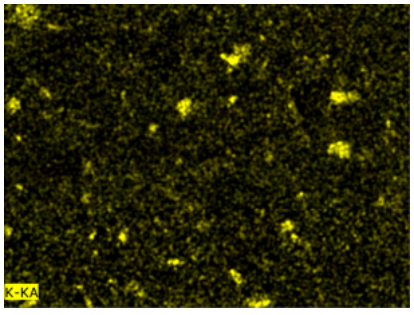

(i) K map

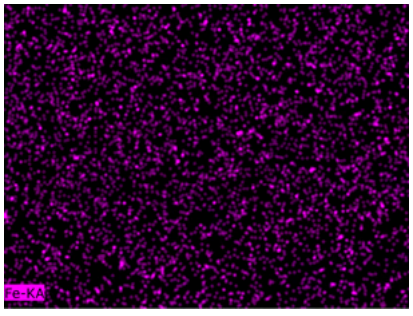

(j) Fe map

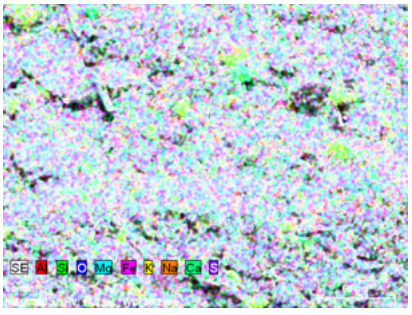

(k) Elemental map

FIGURE D14 EDS Elemental map of Milk Lake precipitate experiment sample. Seed: Kaolinite. Solution: None

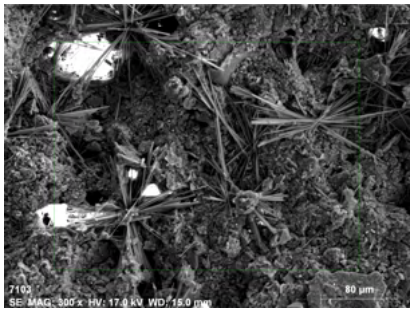

(a) Micrograph

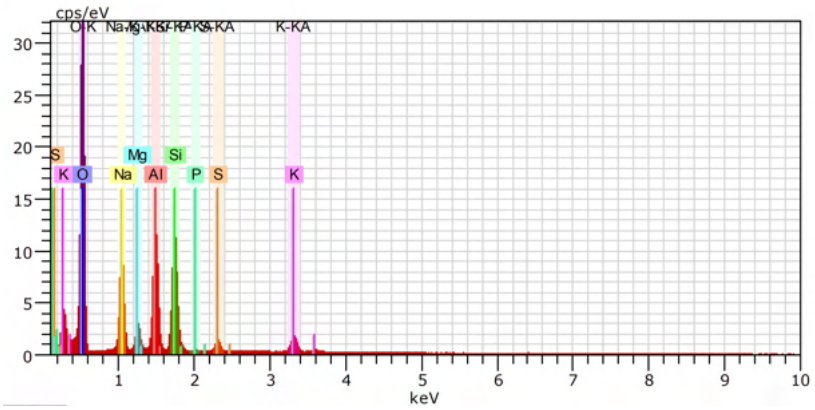

(b) EDS spectrum

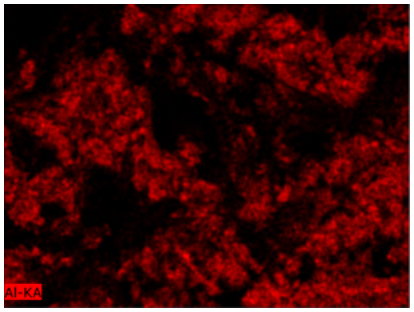

(c) Al map

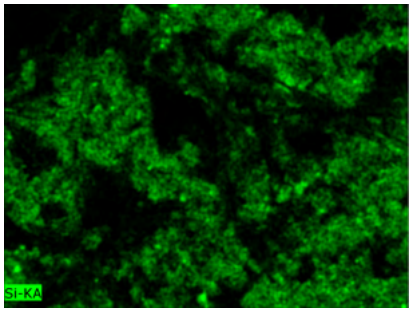

(d) Si map

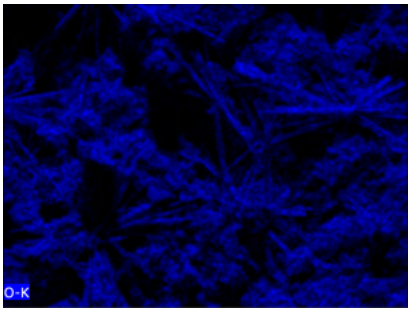

(e) O map

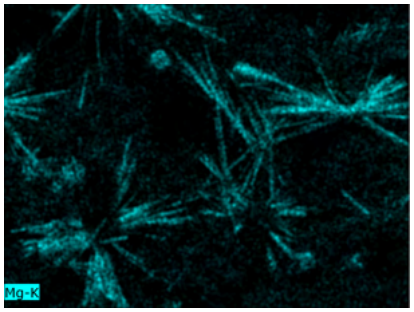

(f) Mg map

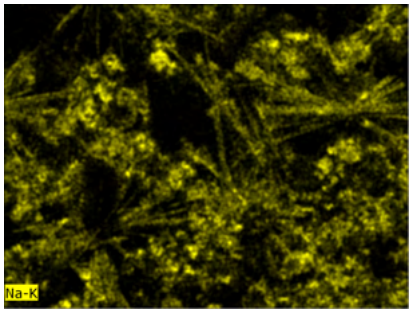

(g) Na map

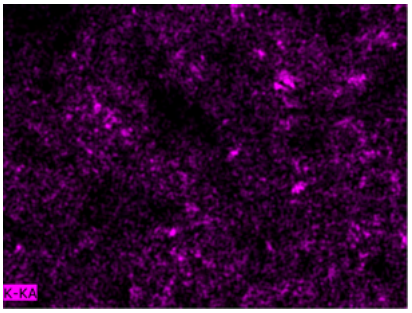

(h) K map

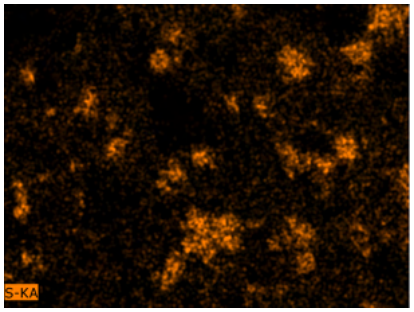

(i) S map

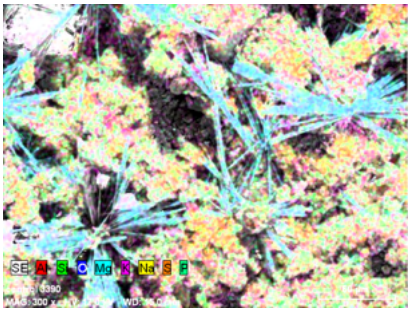

(j) Elemental map

FIGURE D15 EDS Elemental map of Milk Lake precipitate experiment sample. Seed: Kaolinite. Solution: 90% EtOH

E GWB MODELING

E.1 Evaporative Model Plots with Measured Samples

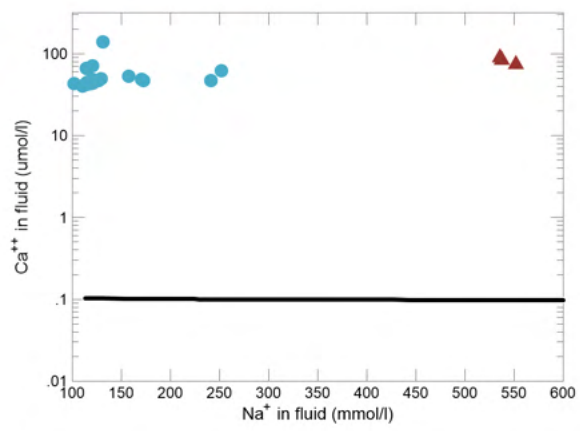

(a) Ca^{2+} vs. Na^{+}

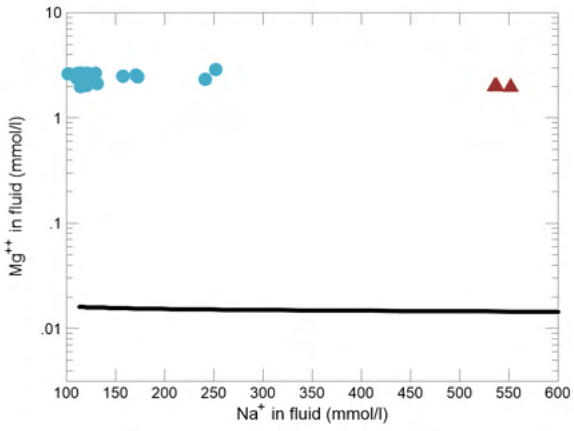

(b) Mg^{2+} vs. Na^{+}

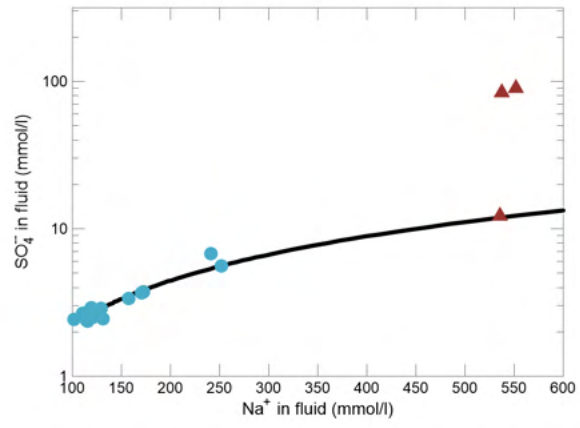

(c) SO_4^{2-} vs. Na^{+}

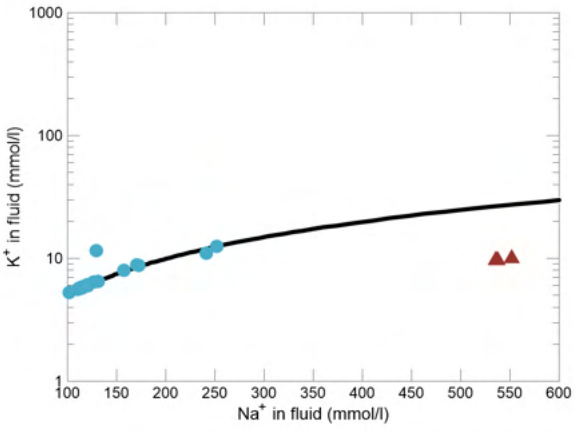

(d) K^{+} vs. Na^{+}

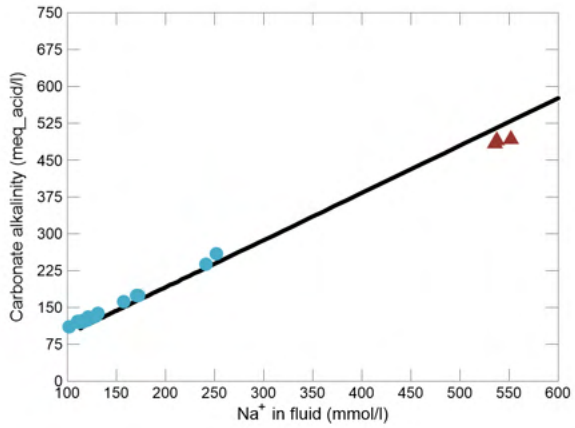

(e) Carbonate Alkalinity vs. Na^+

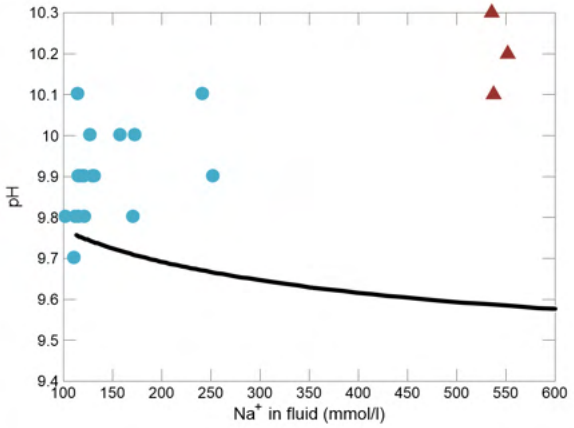

(f) pH vs. Na^+

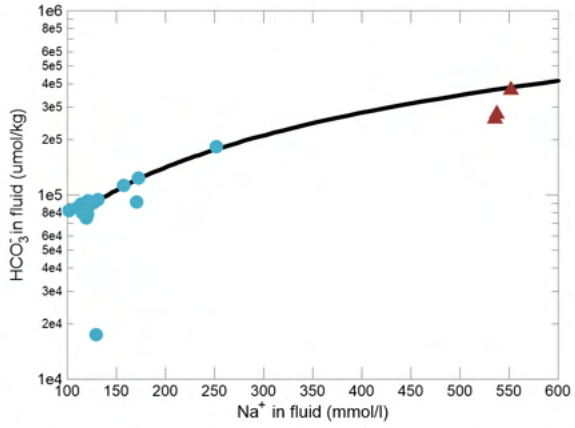

(g) HCO_3^- vs Na^+

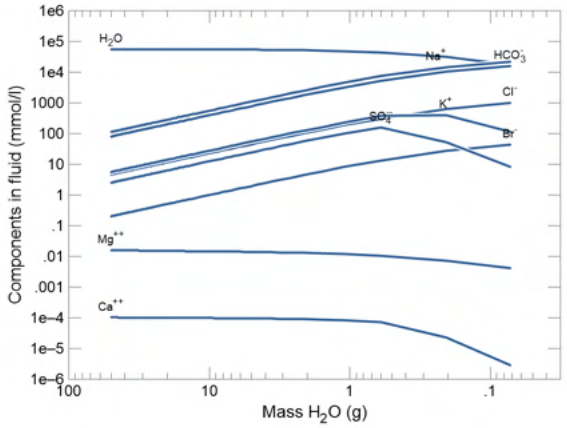

(h) All components in fluid (no measured data)

FIGURE E15 Plot of hypothesised fluid component concentrations over Na^+ (black line). Measured surface water concentrations are plotting with the model line. (Blue circles: Milk Lake; red triangles: Goodenough Lake)